

The Final Report

Title: Inversion of Ionospheric Backscatter Radar data in order to Map and Model the Ionosphere

Principal Investigator:

Peter Dyson Ph.D., Professor

Department of Physics

La Trobe University

Victoria 3086

Australia

Telephone: +61-3-9479-2735

Facsimile: +61-3-9479-1552

E-mail: p.dyson@latrobe.edu.au

Contract Number: FA5209-05-P-0278

AOARD Reference Number: AOARD-54011

AOARD Program Manager: Misoon Mah, Ph.D.

Period of Performance: 10-Feb-05 – 10-Apr-06

Submission Date: 17 Aug 2006

Report Documentation Page			Form Approved OMB No. 0704-0188		
Public reporting burden for the collection of information is estimated to average 1 hour per response, including the time for reviewing instructions, searching existing data sources, gathering and maintaining the data needed, and completing and reviewing the collection of information. Send comments regarding this burden estimate or any other aspect of this collection of information, including suggestions for reducing this burden, to Washington Headquarters Services, Directorate for Information Operations and Reports, 1215 Jefferson Davis Highway, Suite 1204, Arlington VA 22202-4302. Respondents should be aware that notwithstanding any other provision of law, no person shall be subject to a penalty for failing to comply with a collection of information if it does not display a currently valid OMB control number.					
1. REPORT DATE 23 AUG 2006		2. REPORT TYPE Final Report (Technical)		3. DATES COVERED 01-02-2005 to 01-04-2006	
4. TITLE AND SUBTITLE Inversion of Ionospheric Backscatter Radar data in order to Map and Model the Ionosphere			5a. CONTRACT NUMBER FA520905P0278		
			5b. GRANT NUMBER		
			5c. PROGRAM ELEMENT NUMBER		
6. AUTHOR(S) Peter DYSON			5d. PROJECT NUMBER		
			5e. TASK NUMBER		
			5f. WORK UNIT NUMBER		
7. PERFORMING ORGANIZATION NAME(S) AND ADDRESS(ES) La Trobe University, La Trobe University, Victoria 3086, AUSTRALIA, AU, 3086			8. PERFORMING ORGANIZATION REPORT NUMBER AOARD-054011		
9. SPONSORING/MONITORING AGENCY NAME(S) AND ADDRESS(ES) The US Resarch Labolatory, AOARD/AFOSR, Unit 45002, APO, AP, 96337-5002			10. SPONSOR/MONITOR'S ACRONYM(S) AOARD/AFOSR		
			11. SPONSOR/MONITOR'S REPORT NUMBER(S)		
12. DISTRIBUTION/AVAILABILITY STATEMENT Approved for public release; distribution unlimited					
13. SUPPLEMENTARY NOTES					
14. ABSTRACT 14. ABSTRACT Novel solution methods are investigated for electromagnetic ray-tracing models and validation with data from the advanced TIGER (Tasman International Geospace Environment Radar) OTHR (Over-the-Horizon-Radar) Facility.					
15. SUBJECT TERMS					
16. SECURITY CLASSIFICATION OF:			17. LIMITATION OF ABSTRACT	18. NUMBER OF PAGES 55	19a. NAME OF RESPONSIBLE PERSON
a. REPORT unclassified	b. ABSTRACT unclassified	c. THIS PAGE unclassified			



LA TROBE
UNIVERSITY

Department of Physics
Faculty of Science, Technology and
Engineering

UNCLASSIFIED

La Trobe University Research Report

**Inversion of
Ionospheric Backscatter Radar Data
in order to
Map and Model the Ionosphere.**

Peter L. Dyson, Department of Physics

AOARD Research Contract AOARD-05-4011
Final report

UNCLASSIFIED

Final Report on AOARD Research Contract AOARD-05-4011

Project Title: Inversion of Ionospheric Backscatter Radar Data in order to Map and Model the Ionosphere.

Principle Investigator: Prof Peter L. Dyson
Department of Physics
La Trobe University
Victoria
AUSTRALIA

Project Aims:

1. To develop a 2-D High Performance Computing grid point model of the ionosphere in the region of the Tasman International Geospace Environment Radar (TIGER) coverage area. The grid point model will be 2-D in ground range and height, and each grid point will specify ionospheric layer parameters determined from real TIGER ground scatter data using a new inversion technique we have developed. This modelling effort will help to improve our understanding of ionospheric structure on global scales, including gradients in electron density, the occurrence of high-latitude ionospheric troughs and sporadic E, and the associated generation of ionospheric irregularities.
2. To extend the 2-D grid point model to a 3-D grid point model of the ionosphere within the footprint of TIGER. TIGER routinely records echoes on 16 different beam directions so by applying the 2-D grid point approach to each of the beams a 3-D description of the ionosphere may be achieved. We have also developed a 3-D analytic ray tracing technique (not yet published) that can be applied to the 3-D grid point ionospheric model to further test the integrity of the inversion results.

Performance against Projected Milestones:

First Quarter	<u>Milestones:</u> <ul style="list-style-type: none">• Synthesize TIGER Backscatter results using inversion technique• Develop a 2-D HPC grid point model for the E layer	<u>Outcome</u> COMPLETED COMPLETED
Second Quarter	<u>Milestones:</u> <ul style="list-style-type: none">• Develop a 2-D HPC grid point model for the F1 layer	COMPLETED
Third Quarter	<u>Milestones:</u> <ul style="list-style-type: none">• Develop a 2-D HPC grid point model for the F2 layer• Determine the accuracy of the 2-D HPC grid point model	COMPLETED COMPLETED
Fourth Quarter	<u>Milestones:</u> <ul style="list-style-type: none">• Develop a 3-D HPC grid point model• Synthesize TIGER Backscatter results using 3-D HPC SMART• Compare the synthesized results to the real results	COMPLETED - PROTOTYPE DEVELOPED COMPLETED - PROTOTYPE DEVELOPED COMPLETED - PROTOTYPE DEVELOPED

Outcomes:

As indicated in the table showing performance against projected milestones, the project aims have been achieved. In particular the extension of the analysis techniques to three dimensions has been developed and tested in prototype form, but importantly all the software tools that we set out to develop have been developed so that the backscatter inversion techniques can now be applied in further developments such as those outlined in the attached white page on a proposed follow-on project.

The following were proposed as outcomes in the work Plan:

Outcome	Detail
Conference Presentations and Papers	Present papers at one national and two international conferences. Submit at least one paper for refereed publication.
Grants Submitted and/or Received	Submit at least one application for government grant and industry funding for TIGER related research

The following were the actual achievements:

1. Papers (copies attached as Appendices)

- 1.1. Dyson, P. L., M. L. Parkinson, M. Conde and J. C. Devlin.
New Investigations of Magnetosphere-Ionosphere-Thermosphere processes and their Impact on Space Weather.
5th NSSA National Space Science Conference, Melbourne, Australia, pp 1-17, 14-16 September, 2005. ISBN: 0 86459 3740. (Refereed Conference Paper National/International Conference)
- 1.2. Norman R. J. and P.L. Dyson and M. L. Parkinson.
Inversion of HF radar backscatter data in order to map and model the ionosphere.
SuperDARN 2005 Workshop, Ambleside, UK, 16-20 May, 2005. (International Conference).
- 1.3. Norman R. J. and P.L. Dyson and M. L. Parkinson.
Mapping the Ionosphere using a HF Radar Backscatter Inversion Technique.
WARS06 (Workshop on Applications in Radio Science), Leura, Australia, 8 pages, 15-17 February, 2006. (Accepted for publication in proceedings as a refereed paper. WARS06 is a national conference).
- 1.4. Norman, R. J. and P.L. Dyson.
HF Radar backscatter inversion technique.
Radio Sci., (In Press) January 2006. (Refereed journal publication).

2. Grants submitted

- 2.1. Title: *A consolidated approach to ionospheric studies with digital radar systems*
PIs: Dyson and Devlin, La Trobe University, Australia
Lester, Leicester University UK
Bristow, University of Alaska Fairbanks, USA
Grant Body: Australian Research Council
Status: Unsuccessful
- 2.2. Title: *Investigations of Space Weather and the Mesosphere using the TIGER Radar*
CI: Dyson, La Trobe University, Australia
Grant Body: Australian Antarctic Science Program
Status: Awarded A\$17,000 for 2006/07. Project approved for 5 years, funding to be requested on an annual basis.

In summary, the proposed outcomes have been achieved.

Prof Peter L. Dyson
Principle Investigator

Appendix 1

Dyson, P. L., M. L. Parkinson, M. Conde and J. C. Devlin.

New Investigations of Magnetosphere-Ionosphere-Thermosphere processes and their Impact on Space Weather.

5th NSSA National Space Science Conference, Melbourne, Australia, pp 1-17, 14-16 September, 2005. ISBN: 0 86459 3740. (Refereed Conference Paper National/International Conference)

New Investigations of Magnetosphere-Ionosphere-Thermosphere processes and their Impact on Space Weather

Peter L. Dyson^{1,2}, Murray L. Parkinson², M. Conde² and J. C. Devlin³

¹*CRC for Satellite Systems*

²*Department of Physics*

³*Department of Electronic Engineering*

La Trobe University, VIC 3086

AUSTRALIA

Summary: Space weather impacts on some important modern technologies, particularly those that depend on satellites.

The La Trobe Space Physics Research Group studies the basic physical causes of space weather phenomena in geospace, the interface between Earth and interplanetary space. The investigations are based primarily on three experimental techniques: the Tasman International Geospace Environment Radar (TIGER) dual HF radar system; optical spectrometers used to study auroral and airglow emissions; and GPS tomography using the Australian satellite FedSat. Future plans include development of rocket instruments to be flown from Woomera.

This paper will first present a brief overview of some relevant aspects of solar wind-magnetosphere-ionosphere coupling that are the main drivers of space weather in geospace. The La Trobe research program will be described and recent research results of storm-related structure in the plasmasphere, sub-auroral motions and thermospheric wind fields will be presented and discussed. Finally, future research directions will be described.

Keywords: space weather, aurora, magnetic storm, geospace, HF radar, SuperDARN, ionospheric tomography, Fabry-Perot interferometer.

Introduction

Space weather refers to the influences some important conditions on the Sun and in the solar wind have on the magnetosphere, ionosphere and thermosphere. This solar-terrestrial environment, also called geospace, is dominated near the Earth by the interaction of the particles, fields, and radiation environment from the Sun with Earth's space plasma environment and upper atmosphere. Emissions from the Sun impact on the Earth's outer atmosphere producing a variety of effects including large scale disturbances in the Earth's magnetic field and the aurora. While x-rays and high energy particles generated by solar flares travel to the Earth in minutes, other emissions such as coronal mass ejections and features in the solar wind take up to several days.

Space weather impacts on some important modern technologies and particularly those that depend on satellites: long-distance communications (e.g. broadcasts TV, radio, telephone and internet); GPS navigation and position location; remote sensing and weather forecasting. Energetic particles associated with space weather events can damage satellite electronics

causing satellite malfunction or failure, and large magnetic field fluctuations and related currents, electric fields and plasma motions in the ionosphere and magnetosphere also produce significant effects, such as disruption of radio communications and over-the-horizon radar, and reduced accuracy in GPS navigation, and nanotechnology lithography. Many detailed aspects of space weather phenomena are poorly understood, limiting our ability to predict their occurrence and impact.

The solar wind plasma carries with it the Interplanetary Magnetic Field (IMF) that interacts strongly with Earth's magnetic field, confining it in space, particularly on the dayside where the magnetopause is formed at the pressure balance between the solar wind and the Earth's magnetic field (Fig. 1). Under quiescent solar wind conditions the magnetopause forms at $\sim 10 R_e$ (where R_e is the radius of the Earth, ~ 6300 km). During disturbed conditions the magnetopause moves closer to Earth, to $\sim 6R_e$, or even closer during very large events.

The solar wind is rarely steady for long periods of time and the IMF direction can change back and forth between having a northward component and southward component, as shown in Fig. 1. When the IMF is northward, its direction perpendicular to the equatorial plane on the dayside of the Earth is the same as the direction of the terrestrial magnetic field. However, when the IMF is southward the two field directions are opposite and IMF field lines can connect directly to terrestrial field lines, dramatically increasing the coupling of energy from the solar wind into the magnetosphere and consequently into the lower ionosphere and thermosphere. The coupling is not restricted to magnetic energy; it includes the coupling of solar wind plasma into the terrestrial environment. Of course the interaction is not restricted to the dayside as is shown in Fig. 1, which only shows a cross-section perpendicular to the ecliptic. The solar wind-magnetosphere interaction occurs over the three spatial dimensions and Fig. 2 shows that the result is a complex system characterized by different regions of fields, currents and plasma.

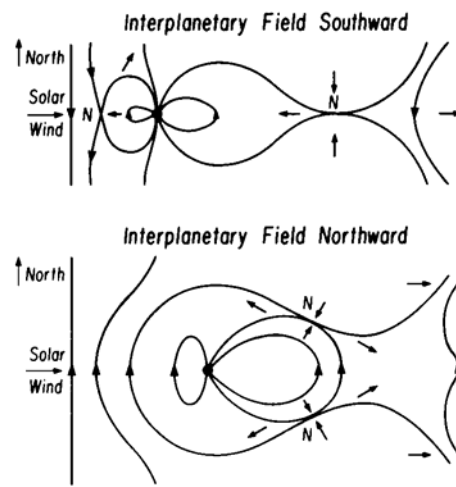


Fig. 1: The interaction between the Interplanetary Magnetic Field (IMF) and Earth's magnetic field in a plane perpendicular to the ecliptic (after [1]).

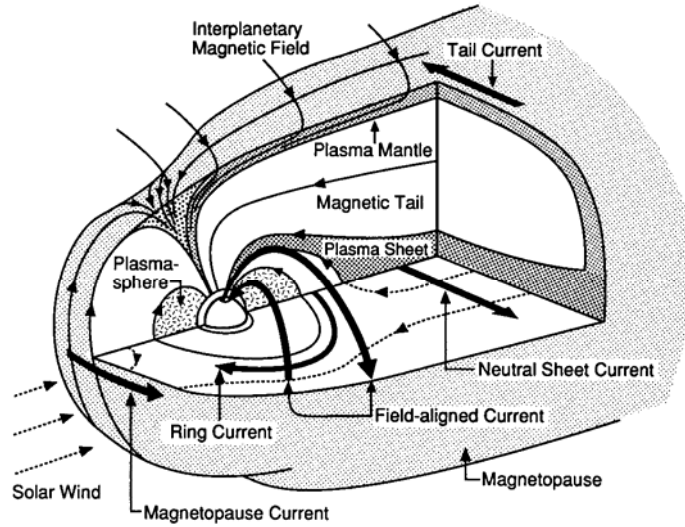


Fig. 2: Schematic of the magnetosphere showing currents, fields and plasma regions (after [1]).

Of specific interest here is that the field lines throughout the vast region of the magnetosphere that is most affected, connect back to high latitudes on the Earth's surface. As a result, at heights of 90 – 1000 km, it is the high latitude ionosphere and thermosphere that are affected most directly by the solar wind's interaction with Earth, and therefore it is at these latitudes that many of the near-earth space weather systems, such as the aurora, generally occur. By studying these high latitude regions we learn not just about their response to changing space weather, but about the processes that transfer energy from the solar wind to the Earth's environment. This is essential information for space weather prediction services.

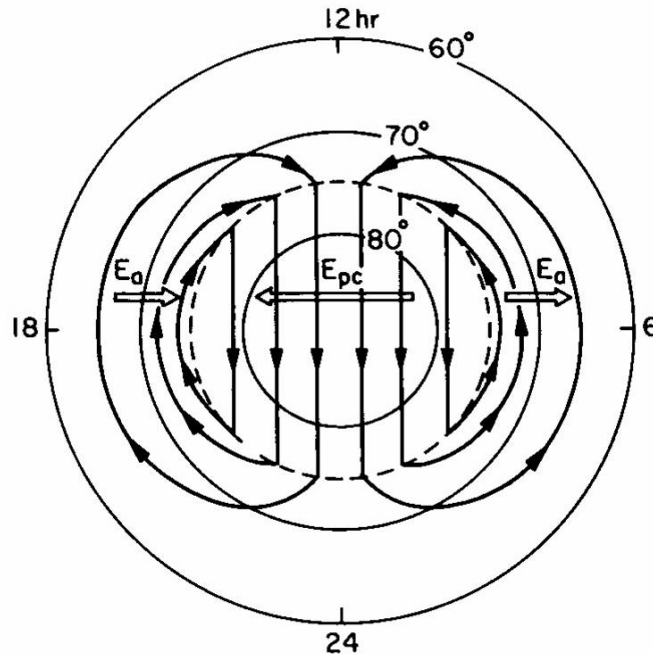


Fig. 3: Representation of ionospheric electric fields in the northern hemisphere polar cap and auroral zone, as well as the resultant plasma flow (after [2]).

A major feature of the high latitude ionosphere is the development of convection cells in the ionosphere in which the ionospheric plasma is transported across the poles from the dayside to the nightside with the return flow at lower latitudes (Fig. 3). The convection comes about through $E \times B$ drift of the plasma caused by a dawn-to-dusk electric field set up across the magnetosphere by the solar wind interaction. This field is conducted down the magnetic field lines to the ionosphere, and coupled with the almost vertical magnetic field at high latitudes, produces significant horizontal $E \times B$ convection in which the plasma, which in the ionospheric F-region at ~ 300 km altitude, reaches speeds as high as 1–2 km/s. Changes in the IMF can produce large scale changes in ionospheric convection that occur within minutes of the IMF changes reaching the magnetopause. Collisions between the ions and neutrals produce similar flow structures in the neutral thermosphere above 100 km which are superimposed on the tidal flows produced by solar heating of the atmosphere.

Many other space weather processes occur in the thermosphere and ionosphere, including particle precipitation that produces the aurora, electrojet currents that flow in the E-region of the ionosphere and produce magnetic disturbances on the ground. These disturbances can also trigger atmospheric gravity waves that propagate to low latitudes; field-aligned currents that flow between the magnetosphere and the ionosphere; and flow channels that form as part of the detailed structure of the convection flows.

The aurora is visually spectacular but can also be observed at wavelengths outside the visible region. Fig. 4 is an observation in the far ultraviolet made by the IMAGE satellite. The aurora is seen to form an oval around the magnetic pole, varying in intensity and latitudinal extent with local time. The ionospheric convection pattern overlays the oval and the enclosed polar region and much current research is aimed determining and understanding the details of the correspondence between the aurora, the convection and other space weather processes, such as those listed in the previous paragraph.

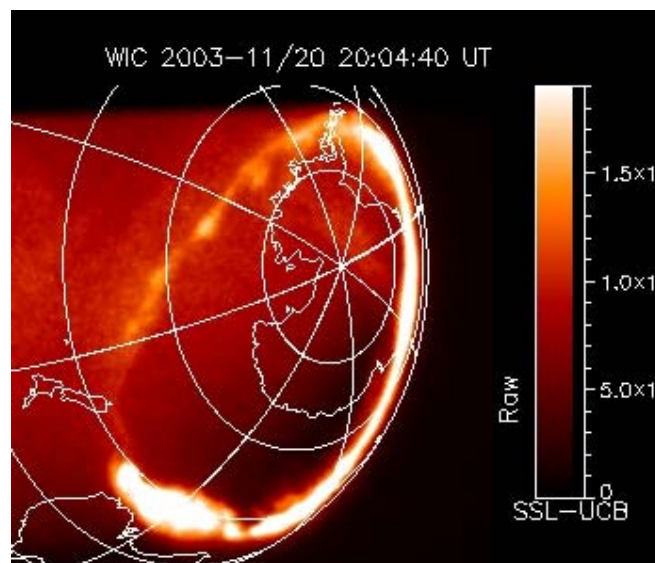
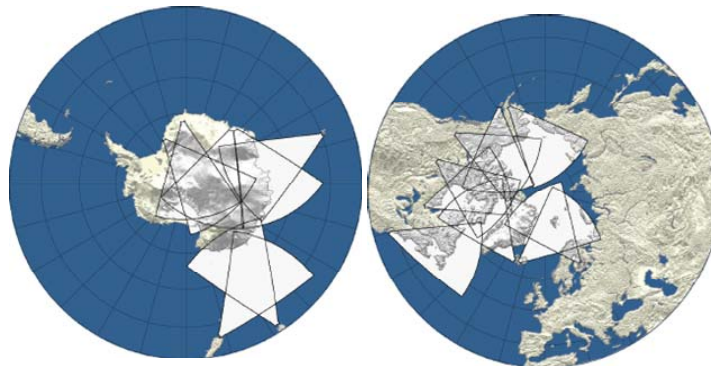


Fig. 4 The aurora australis photographed by the Far UV Imager on the IMAGE satellite (http://son.nasa.gov/tass/aurorafriends/sat_image.htm)

To understand these processes ultimately requires coordinated studies using a world-wide network of satellite and ground based techniques that invariably involve international collaboration. Obviously instruments that measure details of the flow structures in the plasma and neutral atmosphere at high latitudes will play key roles in addressing the gaps in our understanding of space weather processes because they can be used to investigate the development and subsequent decay of many of the phenomena. In this paper we briefly describe the instrumental techniques being used and proposed by the Space Physics Research Group at La Trobe University in our studies of geospace. Some recent results are also presented.

The Tasman International Geospace Environment Radar (TIGER)

TIGER is a dual HF radar system of the Super Dual Auroral Radar Network (SuperDARN) type [3], [4] and in fact is a component of the SuperDARN network of radars [5] that partially ring the north and south polar/high latitude ionospheres (Fig. 5).



*Fig. 5 The SuperDARN network: southern hemisphere (left); northern hemisphere (right).
(after R. Barnes <http://superdarn.jhuapl.edu/index.html>)*

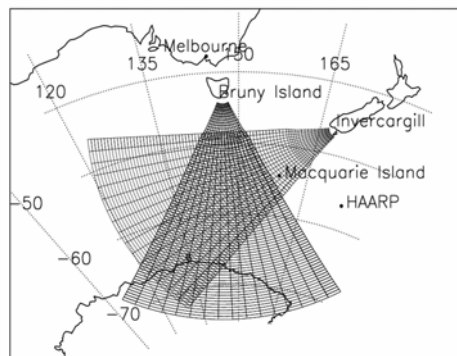


Fig. 6 TIGER locations and radar footprints (Courtesy R. Healy).

One TIGER radar is located on Bruny Island, Tasmania, the other near Invercargill, New Zealand (Fig. 6). An aspect of the high latitude phenomena of interest is that they produce irregularities or turbulence in the ionosphere with structures that are aligned along the Earth's magnetic field lines and which scatter HF radio waves. Strong backscatter, which sends signals back to the radar site, occurs when the HF radio signals become perpendicular to the magnetic field lines (Fig. 7).

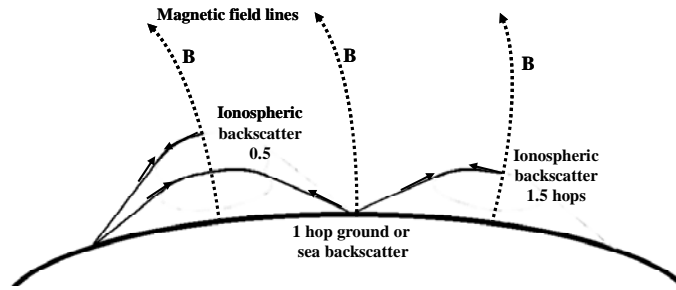


Fig. 7 Ray paths showing ionospheric backscatter from irregularities aligned along the Earth's magnetic field and from the Earth's surface.

Only a small fraction of the radio wave energy is backscattered and at some frequencies and propagation angles the forward propagating wave is reflected by the ionosphere and returns to the ground where it is reflected and so propagates to even greater ranges via a second ionospheric 'hop'. As a consequence ionospheric backscatter can actually be detected from 0.5 and 1.5 hops (and in principle from even greater hops depending on the strength of the backscatter and sensitivity of the radar). Of course some energy is backscattered at each ground reflection and so backscattered signals from the ground, or ocean in the case of the TIGER radars, is also observed. Another source of echoes is backscatter from meteor echoes at ~100 km altitude.

The transmitting antenna for the radars consists of a phased array made up of 16 log-periodic antennas placed on the top of 15 m high towers (Fig. 8). These provide a beam that is $\sim 3.6^\circ$ in azimuth but broad in elevation so that rays launched at different elevations effectively floodlight the ionosphere out to distances of ~ 3000 km. The beam is switched sequentially through 16 steps in azimuth giving an azimuthal coverage of $\sim 52^\circ$ as shown in Fig. 6. Echoes are received on both the transmitting array antenna and a second small array of 4 similar log-periodic antennas placed behind the transmitting array so that the two arrays form an interferometer used to determine echo elevation angle (Fig. 8).



Fig. 8 TIGER Unwin Antennas. 16 element transmit/receive antenna (background) and 4 element receive only antenna (foreground) [Courtesy M. .

The standard mode of operation is for each of the two radars to send out test transmissions over 8–20 MHz and select the frequency that has the greatest range extent of ionospheric scatter and then for the two radars to sweep in azimuth in a synchronised manner, providing complete scans every 1–2 minutes. The radar operating system is very flexible and other modes can be programmed which, say, vary the transmitting frequency, the order or number of azimuthal beams scanned, and/or the time for a complete azimuthal scan.

TIGER provides a unique contribution to SuperDARN. It is the first SD radar pair to be located at comparatively low, sub-auroral latitudes, allowing new studies of these regions that are critically important to understanding what is called the magnetic sub-storm phenomenon, when the Earth's magnetic field in the midnight sector is disturbed and space weather features, such as the aurora, move equatorward, often beyond the field of view of other SuperDARN radars. The generation of related disturbances, such as atmospheric gravity waves, and how they propagate equatorward over Australia are important for regional communications and Australia's surveillance operations using the Jindalee Operational Radar Network (JORN).

Furthermore, the second TIGER radar at Invercargill, named Unwin after a New Zealand scientist who was a pioneer in the development of auroral radar, is one of the few SuperDARN radars that has a stereo capability enabling it to operate on two frequencies simultaneously. Thus it is effectively two radars, and one channel can be synchronised with the Bruny Island (BI) radar, while the other channel is used to conduct special campaigns.

For each echo the radars record the range, angle of arrival, power, line-of-sight velocity (determined from the echo Doppler shift) and Doppler spectral width, usually out to a range of 3000 km. Ionospheric scatter echoes are mostly distinguished from ground or sea scatter by their larger velocities and/or spectral widths. Fig. 9 presents a BI record obtained using one beam direction. It shows the spectral width of echoes as a function of radar frequency. It shows two similar features displaced in range and characterised by different spectral widths so that one appears black and the other red. Each feature consists firstly of a broad region of echoes for which the range hardly changes as the radar frequency is changed. These are due to propagation via what is known as a sporadic-E layer, at about 100 km altitude. The other characteristic of each feature is a broad echo trace at longer ranges that increases in range as the radar frequency is increased. These echoes arise from propagation via the F-region that usually has its peak electron density at ~300 km altitude. The low spectral width echoes (black) are due to 1-hop sea scatter and the large spectral width echoes (red) are due 1.5-hop ionospheric scatter.

A recent discovery made with TIGER is the occurrence of Auroral Westward Flow Channels (AWFC) near the equatorward edge of the auroral oval (Parkinson et al., 2003). Fig. 11 shows observations of such an event by the BI radar. In the radar scan shown on the left of the figure, the echo region from 0.5 hop propagation shows very large line of sight velocities approaching the radar on the eastern side of the scan and receding to the west on the western side. These line of sight components are consistent with a very high speed left flow of ionisation westward across the radar's field of view. The orange and red colours on the eastern side of the scan show that there is latitudinal structure in the strength of the flow, indicating that the flow consists of several high speed channels within a general high speed flow.

The plot on the right of Fig. 11 shows the time evolution of the AWFC as it appears along one radar beam direction. The flow begins very abruptly and last for several hours, although it reduces in speed after about an hour. Magnetometer data from Macquarie Island, which is under the Unwin footprint, shows that the onset of these AWFC channels closely coincides with the onset of magnetic sub-storms [7]. In another study using the King Salmon SD radar in Alaska, we have shown that AWFCs form in both hemispheres (although with asymmetries) as part of the sub-storm phenomenon [8].

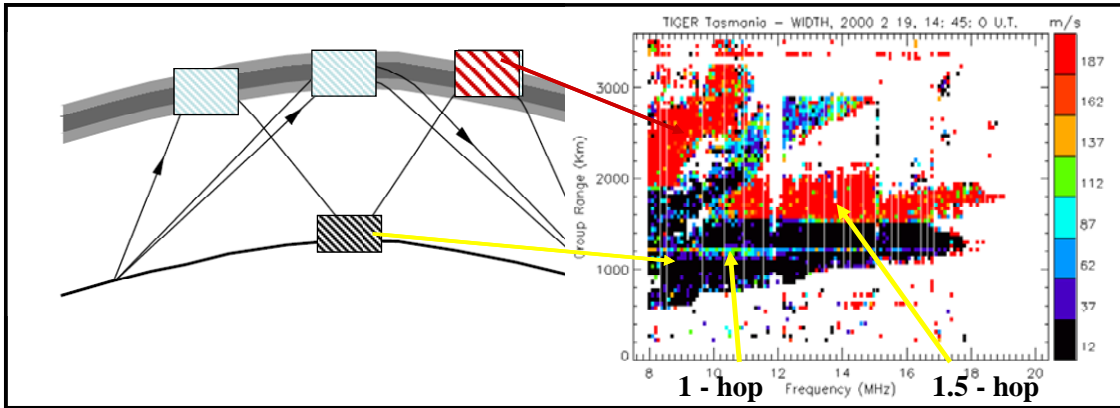
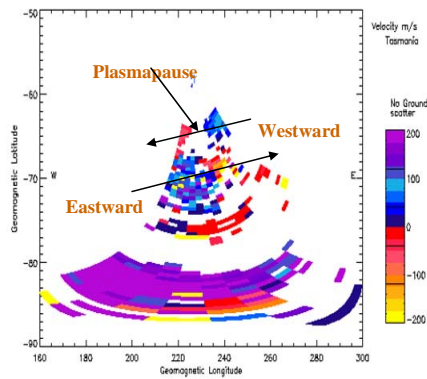


Fig. 9 Observation of 1-hop sea-scatter and 1.5-hop ionospheric scatter. Echo range as a function of radar frequency colour coded according to Doppler spectral width.

Identification of features using
velocity plot

1234 UT, 27 February 2000



Identification of features using
Spectral (Velocity) Widths

1234 UT, 27 February 2000

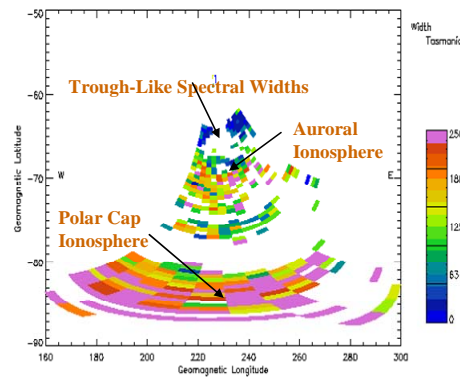


Fig. 10. TIGER Bruny Island radar scan illustrating the use of echo velocity and spectral width to identify different echoing regions.

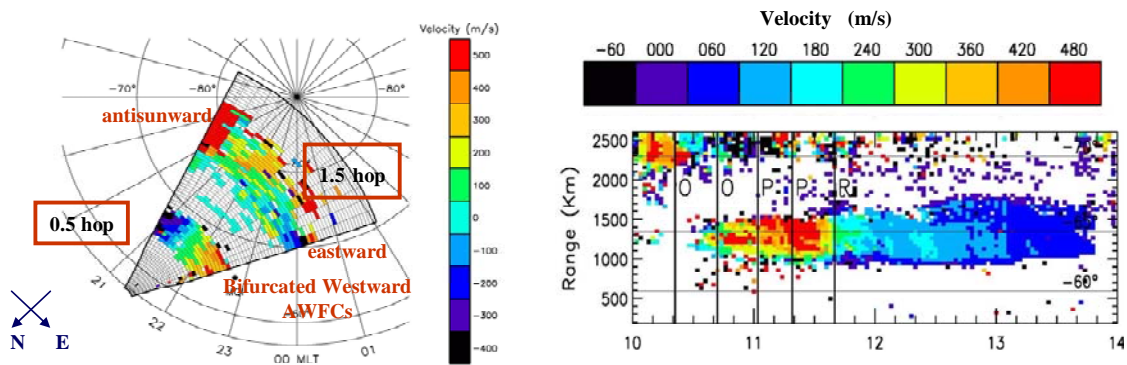


Fig. 11. Observation of an Auroral Westward Flow Channel. Radar scan (left) showing strong structured westward flow in 0.5-hop ionospheric scatter. Single beam observations (right) showing sharp onset of AWFC and duration.

The existence of these AWFCs raises a number of important questions which we are currently investigating:

- What fraction of the total energy dissipation of a substorm is associated with AWFCs?
- How closely synchronised are the start of AWFCs and magnetospheric substorms?
- Can AWFCs precede the start of substorms, and act as a trigger for them?
- Do AWFCs occur under geomagnetic quiet conditions?
- Can we resolve the multiple, filamentary convection structure embedded within AWFCs, and how large are the peak velocities within these filaments?
- What is the relationship between AWFCs, radiation belt particles, and sub-visual auroral red (SAR) arcs?
- What plasma instabilities act within AWFCs, and are AWFCs a source of atmospheric gravity waves?

Other phenomena studied using TIGER include:

- Propagation of atmospheric gravity waves from the auroral region [9]
- ULF waves and micropulsations [10], [11]
- Signatures of magnetospheric boundaries in HF radar data [12], [13]
- Mesospheric winds derived from meteor echoes [14]
- Sea-state.

Future areas of study will concentrate on:

- Identifying signatures of magnetosphere-ionosphere coupling and magnetospheric boundaries.
- Auroral westward flow channels (AWFCs) and their relationship to substorms.
- Ultra-low frequency (ULF; 1-100 mHz) wave fields imaged by the TIGER radars.
- The propagation of ionospheric disturbances from the auroral zone.
- Identifying signatures of severe space weather events.
- Developing methods of determining sea-state
- Identifying tidal motions in the mesosphere-lower thermosphere from the analysis of meteor echoes.

A new generation digital radar is being designed [15], [16]. This will include a receiver on each antenna as opposed to the current two receivers – one for each antenna array. This will provide greater flexibility in operation permitting, for example, beam formation in post processing, so that specific phenomena can be examined and tracked in more detail once their occurrence has been identified

Optical Observations of Thermospheric Winds and Temperatures

The aurora is not the only visible emission from the upper atmosphere. Atomic oxygen in the thermosphere and OH in mesosphere emit sub-visual airglow that can be detected from the ground with appropriate instrumentation. Two important atmospheric parameters are temperature and wind and, if the height of the emitting O and OH is known, the temperature can be determined from the emission line width and the line-of-sight wind component from the Doppler shift of the emission line peak. The same atomic oxygen emissions occur in aurora and airglow so changes in thermospheric wind and temperature can be measured by observing a single emission line. Our research program is directed at observations of these emission lines, providing measurements at atmospheric heights primarily in the range 90–250 km.

A widely used technique for observing airglow and auroral emissions is to use high-throughput (~ 150 -mm plate aperture) Fabry-Perot Interferometers (FPIs) and observe several directions in sequence, e.g. north, south, east, west, all at 30° elevation, and the zenith. We currently operate FPIs in Antarctica at Davis and, at mid-latitudes at Beveridge, near Melbourne. An instrument operated for over a sunspot cycle at Mawson, Antarctica and a new improved replacement instrument is under construction. While many important results have been obtained on the dynamics and thermodynamics of the thermosphere and mesosphere [17]-[22], the spatial resolution of the instruments used has been limited (~ 800 km) and will be greatly improved in the new instrument.

The spatial resolution of the existing instruments is less than desirable because significant variations with much smaller scales than ~ 800 km occur in the high latitude thermosphere. Ground and space based instruments observe vertical wind speeds up to 100 m/s or more, wind shears that reverse the horizontal flow within less than 100 km, and composition perturbations that are equivalent to more than 100 km of vertical transport. Currently these features are too small to be resolved easily by observations or explained by models. These small scales cannot be ignored. Local mixing and intense heat deposition are positive-definite phenomena; there are no corresponding processes to negate their effects through local “un-mixing” or through equally intense local cooling. Their cumulative impact modifies the large-scale structure of the upper atmosphere and ionosphere at altitudes above 100 km, including heights of low Earth orbiting satellites.

To investigate these problems, Conde [23] developed an imaging FPI located in Alaska with a resolution of ~ 100 kms. One result is shown in Fig. 12 which shows the collapse of the thermospheric horizontal wind field during an auroral break-up phase over Alaska. This collapse occurred in a few minutes and was accompanied by a large upward vertical wind. As well as our interest in understanding the processes in the thermosphere during these events, we are also interested in what role such gradients play in modifying the ionosphere.

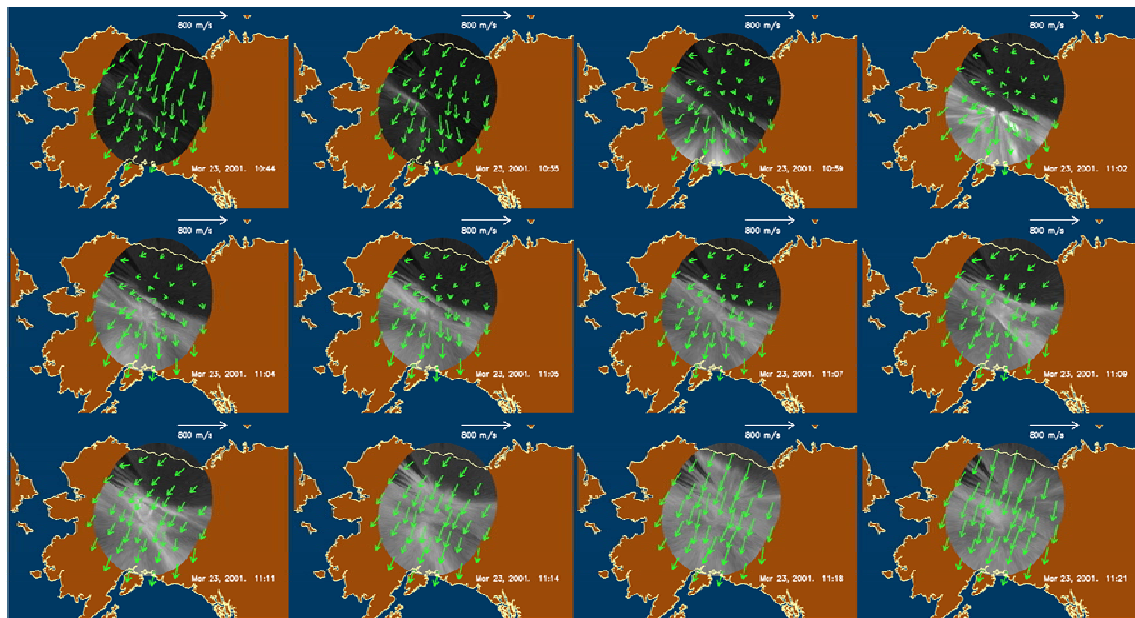


Fig. 12. Observations of thermospheric horizontal winds over Alaska obtained using an imaging Fabry-Perot Interferometer [after 24].

Conde is now developing a new state of the art, hyper-spectral imaging Fabry-Perot optical interferometer (HI-FPI) to be deployed at Mawson, Antarctica (Fig. 13). The all-sky lens is used to obtain a 150° view of the sky. The interference filter has a pass band of a few angstroms and is used to isolate the emission line of interest. A filter wheel provides a set of filters so that different emission lines, coming from different heights in the mesosphere-thermosphere region can be selected. The etalon produces the fringes which are detected by the CCD camera. The separation of the etalon plates is scanned piezoelectrically through a set range so that each camera pixel effectively acts as an individual FPI giving a fringe scan associated with a specific point in the sky.

Based on the operation of the Alaskan system, on *a single night* of active aurora, the new system will acquire 35,000 or more spectra of very high signal-to-noise ratio. By contrast, the simpler FPI that operated at Mawson during the 1980's and 1990's typically gathered only 10,000 to 15,000 noisier spectra over *an entire year*. Thermospheric temperatures are of the order of 1000K and uncertainties are expected to be less than 10K in the zenith, and less than 20K near the edge of the field. Corresponding worst-case line-of-sight wind uncertainties are estimated to be 3 m/s and 6 m/s respectively. Vertical winds in particular may be close to zero at times and the largest winds are over 150 m/s.

We installed an improved FPI at Davis over the 2003-04 summer. Its basic optical elements are similar to that shown in Fig. 13 except that it has a periscope rather than an all-sky lens and the etalon has a fixed spacing. In this system a single CCD image refers the (limited) region of the sky defined by the pointing direction of the periscope. The instrument is capable of quite high time resolution, able to obtain a measurement in tens of seconds compared to minutes for the instrument it replaced. It is also computer controlled and largely operated as a remote instrument from La Trobe via the ethernet.

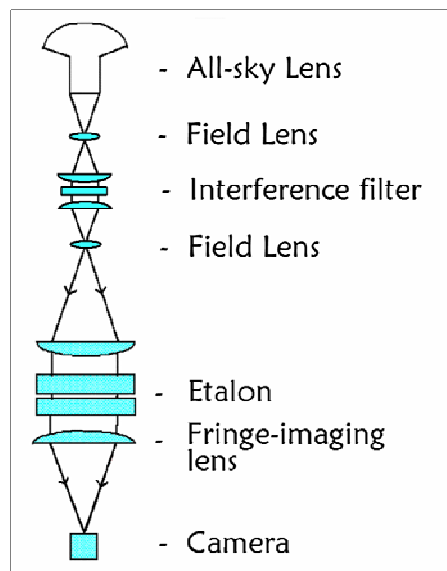


Fig. 13. Schematic of the new hyper-spectral imaging Fabry-Perot optical interferometer (HI-FPI).

The new instrument will be used to study the following phenomena and it will be supported by the current FPI instrument at Davis.

Small-scale (100 km and less) phenomena: These relatively unexplored spatial scales are where the new instrument will excel. Of course there is little point observing such scales without supporting data to show what is driving them. We have an FPI at Davis and both Mawson and Davis are favourably located beneath the field-of-view of the Syowa East SuperDARN (SD) radar, which observes ionospheric convection. This will enable us to address questions such as:

1. What is the response time of the neutral atmosphere to changes in ionospheric convection (as measured by SD), and how does this vary with altitude?
2. At what rate must mechanical energy be supplied to sustain observed horizontal wind shears?
3. Do small-scale space weather disturbances penetrate downward from the F-region into the E-region, or are they excited simultaneously throughout the thermospheric column?
4. What are the relative contributions of local heating and horizontal divergence to driving large vertical wind events? How does this vary with altitude?
5. With the higher spatial resolution and smaller uncertainties of the proposed instrument, are we able to observe auroral excitation of thermospheric gravity waves? If so, can we explain why they appear to propagate preferentially poleward, at least in the middle and upper thermosphere? (eg [25], [26]).

Regional-scale (100-1000 km) phenomena: Greet *et al.* [21] showed that regional structure (hundreds of km) in the neutral wind field could be resolved by combining observations from Mawson and Davis (~650 km apart). With the new instrument, we can expand this work considerably. Topics of interest include:

1. How do the regional-scale wind fields compare with SD convection patterns?
2. Can we observe disturbances propagating in local time – for example in response to a westward travelling surge?
3. Is there a measurable zonal gradient of F-region neutral temperature? If so, under what circumstances?

Satellite Tomography of the Plasmasphere

Soon after satellites were first launched into Earth orbit it was recognised that satellite radio transmissions could be used to determine the Total Electron Content (TEC) along the ray paths from satellites to ground receiving stations. Over the years this has become an important means of studying the ionosphere and the higher altitude plasmasphere. Several methods can be used based on measurements of different radio wave properties such as Faraday rotation, Doppler shift, and the time delay of signal propagation (which is possible with GPS systems). More recently it was recognised that observations from, say, several GPS satellites, can provide a mesh of intersecting ray paths suitable for tomography [27] and this technique has been used by our group to study the response of the ionosphere in the Australian region to space weather impacts [28], [29].

In principle, the use of GPS satellites for tomography provides the capability of determining the 3-D structure of the ionosphere-plasmasphere system out to ~22,600 km, the orbital height of the satellites. However in reality, the plasma density falls off rapidly above and below the F-region ionospheric peak, typically at 250-300 km altitude, so that GPS tomography using ground stations provides excellent detail of the F-region of the ionosphere, but not of the plasmasphere above.

The Australian satellite FedSat (www.crcss.csiro.au/fedsat/), orbits at an altitude of ~ 800 km, well above the F-region peak and so provides an excellent platform for GPS tomography of the plasmasphere which is a region about which little is known of its detailed structure and response to space weather changes such as occur during geomagnetic storms.

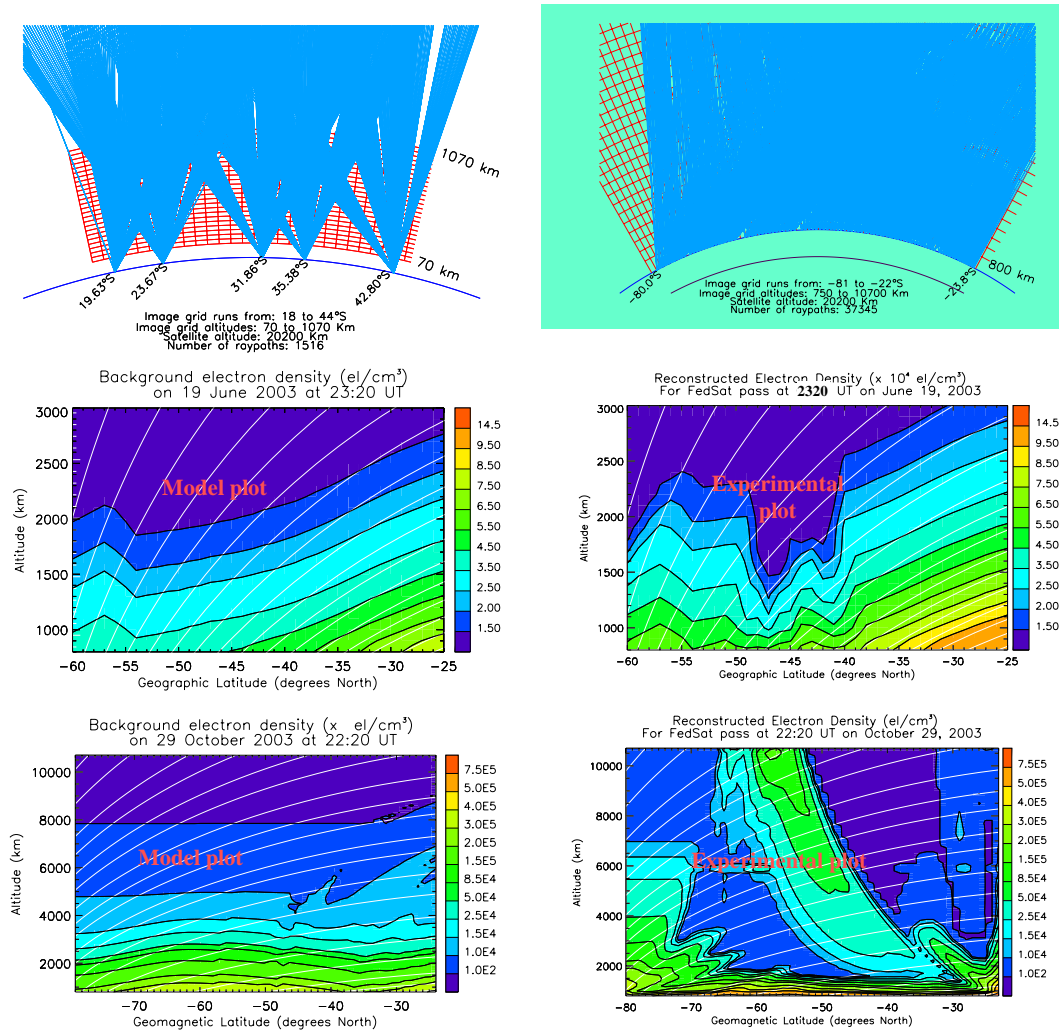


Fig. 14. (Top) GPS ray path grids for plasma tomography using ground stations (left) and FedSat (right).
 (Middle) Structure of plasmasphere during magnetically quiet conditions.
 (Lower) Structure of plasmasphere during magnetically disturbed conditions.
 The white lines represent the Earth's magnetic field lines.

Fig. 14 shows initial results from an ongoing study of the plasmasphere using FedSat [31]. The top panel compares the typical ray grid obtained during a FedSat pass with that obtained using 5 ground stations over Australia. It is evident that the FedSat observations provide a denser grid giving more uniform coverage of the region being investigated. The other two panels show comparisons between FedSat observations of the plasmasphere and model predictions for the same solar geophysical conditions. The model developed by Webb [32], provides a good description of our current knowledge of the detailed structure and behaviour of the plasmasphere. The middle panel shows for relatively undisturbed geophysical and solar conditions, there is quite good agreement between model and observation in the background

structure of the plasmasphere, but the observations show a trough feature not predicted by the model.

The lower panel show a comparison under very disturbed conditions and the observations show quite complicated structures not predicted by the model. In the plasmasphere the plasma is dominated magnetic field effects and so structures can be expected to be field-aligned. There is evidence of this in the observations between 1500 and 4000 km altitude and 50°-70° S. However the plasmasphere is dominated by generally reduced plasma density and an enhancement that stretches upwards across the field lines. This suggests that electric fields are playing a significant role in transporting plasma across the field lines by $E \times B$ drift.

These two examples illustrate our lack of detailed knowledge of the structure and dynamics of the plasmasphere under changing space weather conditions and our FedSat studies have the potential to extend significantly our understanding of this region.

Other Research Developments

Significant research programs are also being undertaken using vertical incident radars (ionosondes) in Antarctica and at La Trobe's Bundoora campus. The Antarctic program is a collaborative program with Dr Ray Morris, Australian Antarctic Division and has included detailed mapping of ionospheric convection at Casey, Antarctica, a polar cap station [34], [32].

The experimental radio studies are supported by ray tracing studies [35], the development of new inversion techniques, including use of FedSat occultation observations to determine ionospheric structure [36].

A new initiative being led by Dr Conde is the planned development of rocket payloads to measure properties of the atmosphere up to 100 km using sounding rockets being developed by the University of Queensland [37].

Conclusions

The complexity of the coupling from the solar wind to Earth's magnetosphere, ionosphere and thermosphere results in a great variety of space weather phenomena that cannot all be studied by any one technique. Progress is dependent on coordinated studies using world-wide networks of satellite and ground based techniques involving different instruments and international collaboration between various scientific groups. In this paper three techniques, HF ionospheric radar, large Fabry-Perot Interferometers, and satellite-to-satellite tomography, used by the Space Physics research Group at La Trobe University, have been described. Some recent results have been described and the leading research questions which each technique can address have been presented.

Acknowledgements

The research programs discussed here have been supported by the following: Australian Research Council, Australian Government's Cooperative Research Centres Program,

Australian Antarctic Science program, US Air Force Office of Scientific Research, Victorian Partnership for Advanced Computing, British Antarctic Survey, and the partners of the TIGER Consortium (La Trobe University, Monash University, University of Newcastle, Australian Antarctic Division, IPS Radio and Space Services, ISR Division of DSTO). Mr Theo' Davies designed the FPI installed at Davis over the 2003-04 summer.

References

1. Kivelson, M. G. and Russell, C. T., *Introduction to Space Physics*, Cambridge University Press, Cambridge, 1995.
2. Kelley, M. C., *The Earth's Ionosphere*, Academic Press, San Diego, 1989.
3. Dyson, P. L. and Devlin, J. C., The Tasman International Geospace Environment Radar, *The Physicist (The Australian Institute of Physics)*, Vol. 37, 48-53, March/April, 2000.
4. Dyson, P. L. and Devlin, J. C., The TIGER Radar - An Extension of SuperDARN to Sub-auroral Latitudes (Invited). *WARS'00 (Workshop on Applications of Radio Science) Proceedings*, (Eds. Dyson and Norman), La Trobe University, 9-31, 2000.
5. Greenwald, R. A., Bristow, W. A., Sofko, G. J., Senior, C., Ceriser, and J.-C., Szabo, A., Super Dual Auroral Radar Network radar imaging of dayside high-latitude convection under northward interplanetary magnetic field: Toward resolving the distorted two-cell versus multicell controversy, *J. Geophys. Res.*, Vol. 100, 19661-19674, 1995.
6. Parkinson, M. L., Pinnock, M., Ye, H., Hairston, M. R., Devlin, J. C., Dyson, P. L., Morris, R. J., and Ponomarenko P., On the lifetime and extent of an auroral westward flow channel (AWFC) observed during a magnetospheric substorm, *Ann. Geophysicae*, Vol. 21, pp. 893–913, 2003.
7. Parkinson, M. L., Dyson, P. L., and Pinnock, M., The importance of auroral westward flow channels in substorm evolution, *Adv. Space Res.*, In Press, 2005.
8. Parkinson, M. L., Pinnock, M., Wild, J. A., Lester, M., Yeoman, T. K., Milan, S. E., Ye, H., Devlin, J. C., Frey, H. U., and Kikuchi, T., Interhemispheric asymmetries in the occurrence of magnetically conjugate sub-auroral polarisation streams, *Ann. Geophysicae*, Vol. 23, pp. 1371–1390, 2005.
9. He, L.-S. , Dyson, P. L., Parkinson, M. L., and Wan, W., Studies of medium scale travelling ionospheric disturbances using TIGER SuperDARN radar sea echo observations, *Annales Geophysicae*, Vol. 22, 4077 – 4088, 2004.
10. Ponomarenko, P.V., Menk, F.W., Waters, C.L., Parkinson, M.L., Dyson, P.L., Observation of ULF waves in vicinity of the plasmopause using SuperDARN TIGER radar *WARS02 (Workshop on Applications of Radio Science) Proceedings*, (Ed. P. Wilkinson) National Committee for Radio Science, Australian Academy of Science, Paper H2, 2002.
11. Ponomarenko, P. V. and. Waters, C. L., The role of Pc1-2 waves in spectral broadening of SuperDARN echoes from high latitudes. *Geophys. Res. Let.*, Vol. 30, No 3, 22-1 to 22-4, 2003.
12. Parkinson M. L., Dyson, P. L., Pinnock, M., Devlin, J. C., Hairston, M. R., Yizengaw, E. and Wilkinson, P. J., Signatures of the midnight open-closed magnetic field-line boundary during balanced dayside and nightside reconnection. *Annales Geophysicae.*, Vol. 20, No 10, 1617-1630, 2002.
13. Parkinson, M. L., Chisham, G., Pinnock, M., Dyson, P. L. and Devlin, J. C., Magnetic local time, substorm, and particle precipitation-related variations in the behaviour of SuperDARN Doppler spectral widths, *Annales Geophysicae*, Vol. 22, 4103 – 4122, 2004.

14. Matthews, D. M., Parkinson, M. L., Dyson, P. L., and Devlin, J. C., Optimising Estimates of Mesospheric Neutral Wind Using the TIGER SuperDARN Radar. *Adv. Space Res.*, (in press), July 2005.
15. Whittington, J., Devlin, J. and Salim, T., Evaluation of Digital Generation and Phasing Techniques for Transmitter Signals of the TIGER N.Z. Radar. *WARS02 (Workshop on Applications of Radio Science) Proceedings*, (Ed. P. Wilkinson) National Committee for Radio Science, Australian Academy of Science, Paper G12, pp 1-4, 2002.
16. Whittington, J., Devlin, J. and Nguyen, M., Digital Stereo Enhancement to the TIGER Radar System. *WARS04 (Workshop on the Applications of Radio Science) Proceedings*, (Ed. P. Wilkinson) National Committee for Radio Science, Australian Academy of Science, Paper G15, pp 1-12, 2004.
17. Conde, M. and Dyson, P. L., Thermospheric Vertical Winds Above Mawson, Antarctica, *J. Atmos. Terr. Phys.*, Vol. 57, 589-596, 1995.
18. Conde, M. and Dyson, P. L., Thermospheric horizontal winds above Mawson, Antarctica, *Adv. Space Res.*, Vol. 16, (5) 41-52, 1995.
19. Dyson P. L., Davies, T. P., Richards, P. G., Parkinson, M. L., Reeves, A. J. and Fairchild, C. E., Thermospheric Neutral Wind at Southern Mid-Latitudes: A Comparison of Optical and Ionosonde $h_m F_2$ Methods, *J. Geophys. Res.*, Vol. 102, No A12, 27,189-27,196, 1997.
20. Greet P. A. and Dyson P. L., Tidal periodicities in observations of the OH(6-2) emission from Mawson, Antarctica. *Adv. Space Res.*, Vol. 24, No 5, 579-582, 1999.
21. Greet P. A., Conde, M. G., Dyson, P. L., Innis, J. L., Breed, A. M. and Murphy, D. J., Thermospheric wind field over Mawson and Davis, Antarctica; Simultaneous observations by two Fabry-Perot spectrometers of $\lambda 630$ nm emission. *J. Atmos. Solar Terr. Phys.*, Vol. 61, No 14, 1025-1045, 1999.
22. Innis, J. L., Greet, P. A., Murphy, D. J., Conde, M. and Dyson, P. L., A large Vertical Wind in the thermosphere at the Auroral Oval/Polar Cap Boundary seen simultaneously from Mawson and Davis, Antarctica. *J. Atmos. Solar Terr. Phys.*, Vol. 61, No 14, 1047-1058, 1999.
23. Conde, M., and Smith, R. W., Phase compensation of a separation scanned, all-sky imaging Fabry-Perot spectrometer for auroral studies, *Appl. Opt.*, Vol. 36, 5441-5450, 1997.
24. Conde, M., and Smith, R. W., Simultaneous Observations of the Aurora and of Non-Uniform Thermospheric Winds, from Poker Flat, Alaska, *Proc. NIPR Symp. Upper Atmos. Phys.*, Vol. 12, 30-38, 1998.
25. Innis, J. L. and Conde M., Thermospheric vertical wind activity maps derived from Dynamics Explorer-2 WATS observations, *Geophys. Res. Lett.*, Vol. 28: 3847-3850, 2001.
26. Innis, I. L. and Conde, M., High-latitude thermospheric vertical wind activity from Dynamics Explorer-2 WATS observations: Indications of a source region for polar cap gravity waves, *J. Geophys. Res.* Vol. 107, No. A8, 10,1029/2001JA009130, 2002.
27. Austen, J. R., Franke, S. J., and Liu, C. H., Ionospheric Imaging Using Computerized Tomography, *Radio Sci.* Vol. 23 No. 3, 229-307, 1988.
28. Yizengaw, E., Moldwin, M., Dyson, P. L., and Immel, T. J., The Southern Hemisphere ionosphere and plasmasphere response to the interplanetary shock event of 29-31 October 2003, *J. Geophys. Res.*, Vol. 110, A09S30, doi:10.1029/2004JA010920, 2005.
29. Yizengaw, E., Dyson, P. L., Essex, E. A., and Moldwin, M. B., Comprehensive ionosphere dynamics study over the Southern Hemisphere during the severe magnetic storm on 31 March 2001, *Ann. Geophys.* Vol. 23, No. 3, 707-721, 2005.
30. Yizengaw, E., Dyson, P., and Essex, E., Tomographic reconstruction of the ionosphere using ground-based GPS data in the Australian region. *WARS04 (Workshop on the*

- Applications of Radio Science) Proceedings*, (Ed. P. Wilkinson) National Committee for Radio Science, Australian Academy of Science, Paper G16, pp 1-9, 2004.
31. Yizengaw, E., Dyson, P. L., Essex E. A., A study of the spatial density distribution in the topside ionosphere and plasmasphere using the FedSat GPS receiver, *Adv. Space Res.*, In Press, 2004.
 32. Webb, P., *A dynamic global model of the plasmasphere*. Ph.D. Thesis, La Trobe University, 2000.
 33. Smith P. R., Dyson, P. L., Monselesan, D. P. and Morris, R. J., Ionospheric Convection at Casey, a Southern Polar Cap Station, *J. Geophys. Res.*, Vol. 103, No A2, 2209-2218, 1998.
 34. Smith, P. R., Dyson, P. L. and Morris, R. J., Comparison of an ionosonde drift model at a single station with polar convection patterns, *J. Geophys. Res.*, Vol. 104, No. A12, 28,089 - 28,099, 1999.
 35. Bennett, J. A., Dyson, P. L. and Norman, R. J., Progress in Radio Ray Tracing in the Ionosphere. *The Radio Science Bulletin*, No 310, 81-91, September 2004.
 36. Norman, R. J., Parkinson, M. L. and Dyson, P. L., Comparing HF Radar Backscatter from the Southern Ocean with Ray-Tracing Results using the IRI model. *WARS04 (Workshop on the Applications of Radio Science) Proceedings*, (Ed. P. Wilkinson) National Committee for Radio Science, Australian Academy of Science, Paper G8, pp 1-10, 2004.
 37. Teakle, P. and Zander, F., Scientific Sounding Rocket Development at the University of Queensland, *Proceedings 5th NSSA Space Science Conference*, this issue, 2005.

Appendix 2

Norman R. J. and P.L. Dyson and M. L. Parkinson.

Inversion of HF radar backscatter data in order to map and model the ionosphere.

Oral Presentation at SuperDARN 2005 Workshop, Ambleside, UK, 16-20 May, 2005. (International Conference).

Inversion of HF radar backscatter data in order to map and model the ionosphere

R. J. Norman, P. L. Dyson

and

M. L. Parkinson



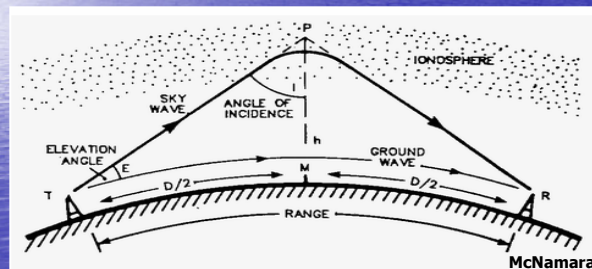
**LA TROBE
UNIVERSITY**

Department of
Physics



Introduction

HF signals propagated via the ionosphere and backscattered from the Earth's surface inherently contain information on the ionospheric structure along the signal ray path.



$$P' = \int_{\text{ray}} \mu' ds$$

$$\mu' = \mu'(N_e, f, f_H, \theta)$$

$$\mu' \approx \mu'(N_e, f)$$

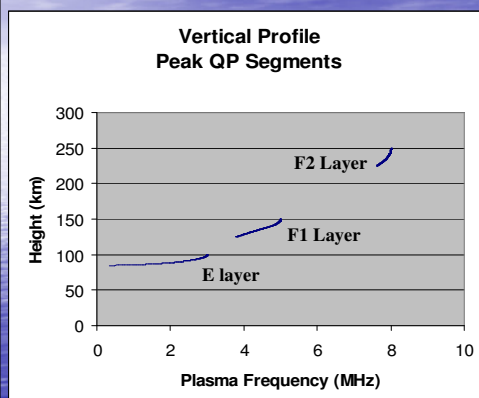
This paper presents a backscatter inversion technique that uses the elevation angle and group path of the received signals.

The Inversion Technique

This initial version is based on describing the vertical structure of the ionosphere in terms of three quasi-parabolic (QP) layers.

QP layers are a convenient mathematical description for a spherically stratified ionosphere because they provide analytical expressions for ray parameters, such as P' , which reduces computation time significantly compared to numerical ray tracing.

Simple QPS 3 Layer model (3 Layers, 5 Segment QPS Ionosphere)

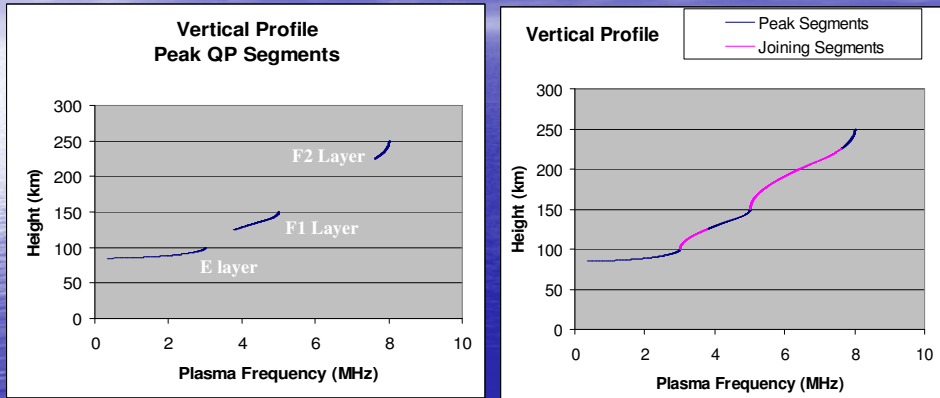


Each layer is described by:

- Critical frequency
- Peak Height
- Semi-thickness

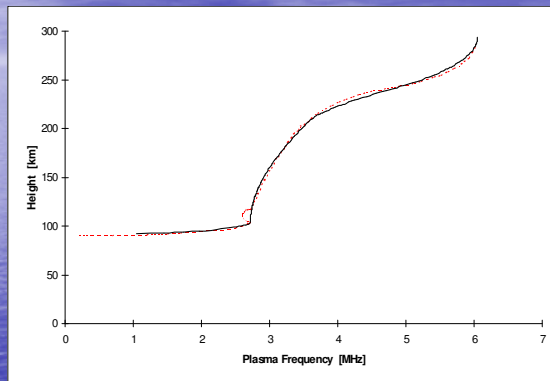
Dyson, P. L. and J. A. Bennett. A model of the vertical distribution of the electron concentration in the ionosphere and its application to oblique propagation studies, *J. Atmos. Terr. Phys.*, **50**, 251-262, 1988.

Simple QPS 3 Layer model (3 Layers, 5 Segment QPS Ionosphere)



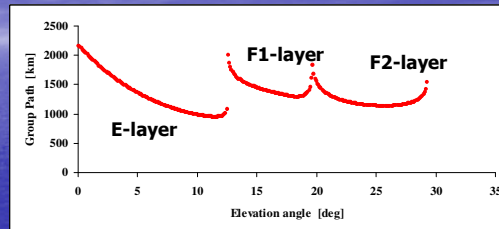
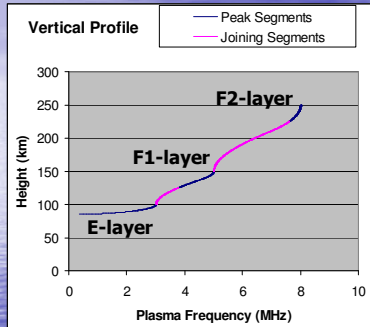
Dyson, P. L. and J. A. Bennett. A model of the vertical distribution of the electron concentration in the ionosphere and its application to oblique propagation studies, *J. Atmos. Terr. Phys.*, **50**, 251-262, 1988.

More Realistic Profiles can be obtained by fitting more QP segments:



Chen, J., J. A. Bennett and P. L. Dyson. Automatic fitting of quasi-parabolic segments to ionospheric profiles with application to ground range estimation for single-station location, *J. Atmos. Terr. Phys.*, **52**, 277-288, 1990.

Relationship between Group Path and Elevation Angle on a single frequency



Each layer is described by:

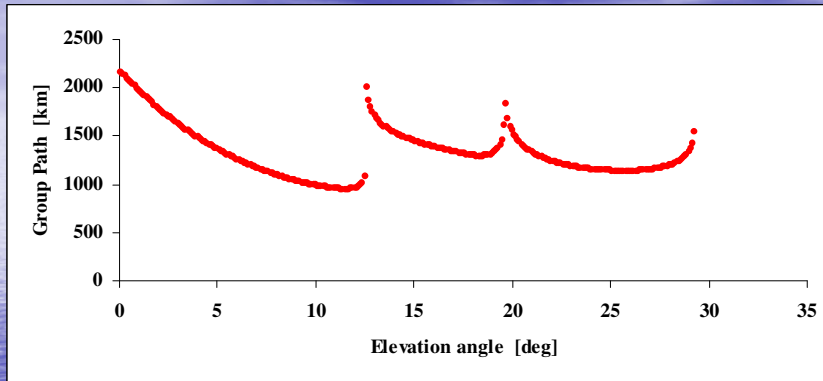
- Critical frequency
- Peak Height
- Semi-thickness

Hence inversion requires at least 3 points per layer

Basic Theory

- The inversion technique requires n (where $n > 2$) data points from each of the layer echo traces, where the group paths P'_1, P'_2, \dots, P'_n are chosen corresponding to the n elevations E_1, E_2, \dots, E_n respectively.
- There exist explicit equations for the Group path expressed in terms of the layer parameters and the initial elevation angle.
- The method then sets out to find a set of values for the layer parameters, which yield to within a specified accuracy, to the data points chosen.

INVERSION OF SYNTHESIZED (P, E)



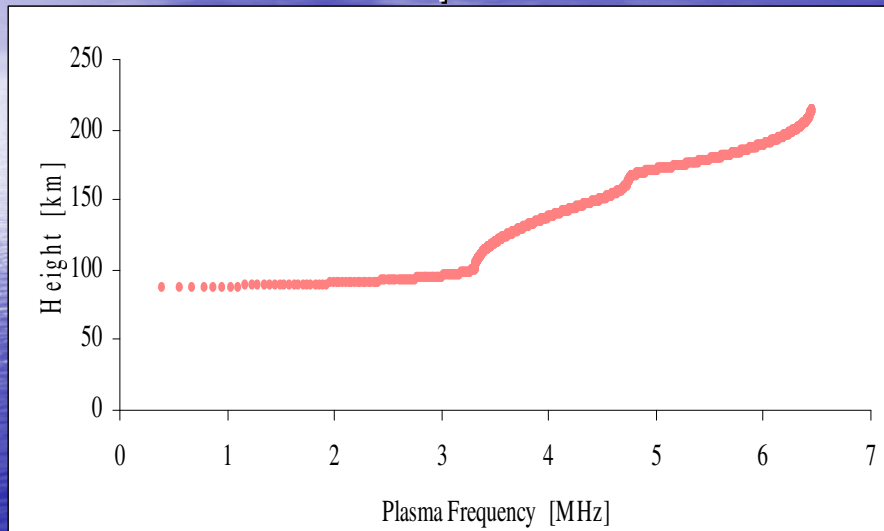
E layer $E = 3.32$ MHz, $y_m E = 14$ km, $h_m E = 101 + r_0$ km
 F1 layer $F1 = 4.75$ MHz, $y_m F1 = 43$ km, $h_m F1 = 164 + r_0$ km
 F2 layer $F2 = 6.45$ MHz, $y_m F2 = 68$ km, $h_m F2 = 214 + r_0$ km
 where $r_0 = 6370.0$ km (the radius of the Earth).

Data Point	Elevation angle [deg]	Group Path [km]
E layer		
1	5.0	1361.49009944569
2	7.0	1168.63887920563
3	9.0	1033.35342695743
	12.0	
F1 layer		
	[deg]	[km]
1	19.0	1404.10692246982
2	19.2	1348.36189670986
3	19.4	1319.28979088134
	19.7	
F2 layer		
	[deg]	[km]
1	22.0	1238.53947948455
2	23.0	1187.14934478616
3	24.0	1155.70487464130
	29.3	

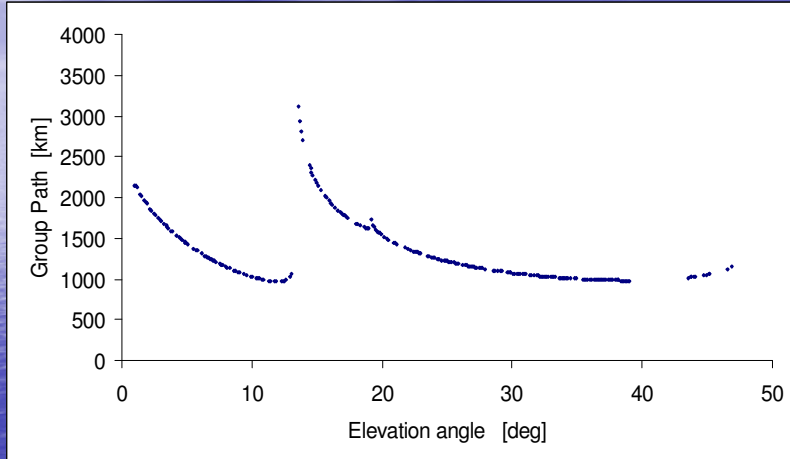
Table 2 Shows the convergence of the E layer parameters to the correct result after each iteration

	E Layer Iteration No.				
	1	2	3	4	5
foE [MHz]	3.253448	3.344400	3.319285	3.319999	3.320000
ymE [km]	13.00000	14.53291	13.98480	13.99999	14.00000
hmE [km]	91.00000	101.1981	100.9853	101.0000	101.0000
P'_{c1} [km]	1255.018	1359.362	1361.448	1361.490	1361.490
P'_{c2} [km]	1070.978	1166.943	1168.593	1168.639	1168.639
P'_{c3} [km]	943.9176	1031.923	1033.308	1033.353	1033.353
$\Delta P'_1$ [km]	106.4718	2.12810	4.188E-02	2.971E-05	2.87E-09
$\Delta P'_2$ [km]	97.66112	1.69550	4.579E-02	3.412E-05	1.56E-10
$\Delta P'_3$ [km]	89.43584	1.43042	4.553E-02	3.631E-05	-1.39E-09

Resultant Ionospheric Profile



Inversion Technique with IRI model



(P' , E) obtained using 3-D numerical ray tracing

E layer After 5 Iterations

P' [km]	Error in P' [km]	
1361.49009944340	2.29E-009	
1168.63887920547	1.57E-010	
1033.35342695882	-1.38E-009	
foE = 3.32 MHz	ymE = 14.0 km	hmE = 101.0 km

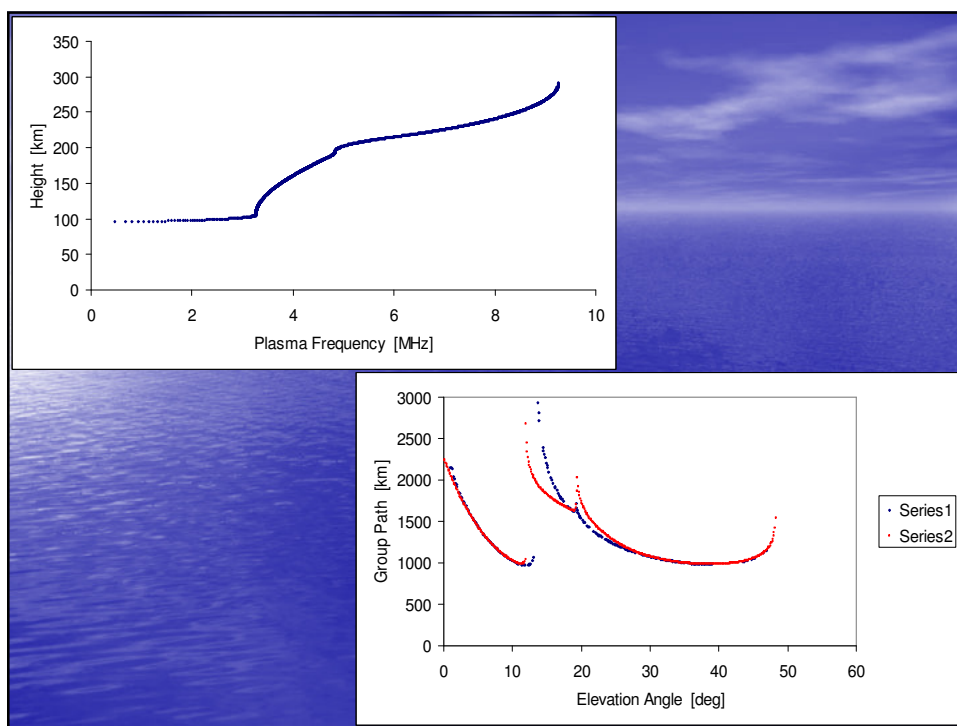
F1 layer After 6 Iterations

P' [km]	Error in P' [km]	
1319.28979085530	2.60E-008	
1348.36189671118	-1.32E-009	
1404.10692269213	-2.22E-007	
foF1 = 4.75 MHz	ymF1 = 43.0 km	hmF1 = 164.0 km

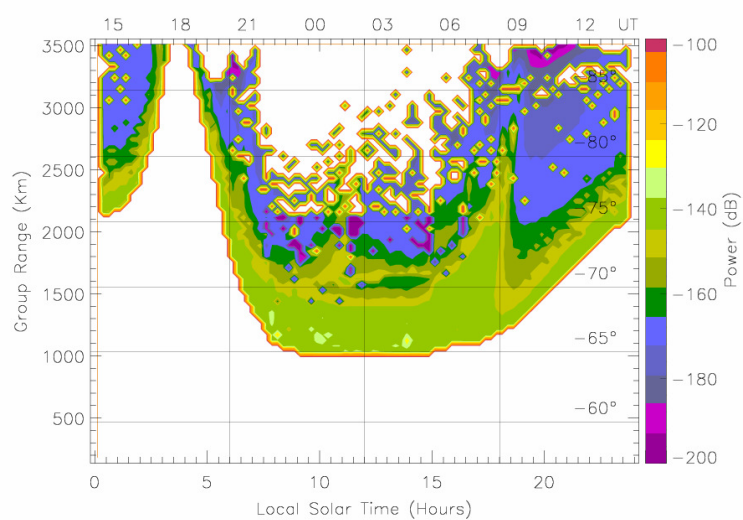
F2 layer After 5 Iterations

P' [km]	Error in P' [km]	
1238.53947945607	2.85E-008	
1187.14934476562	2.05E-008	
1155.70487462347	1.78E-008	
foF2 = 6.45 MHz	ymF2 = 68.0 km	hmF2 = 214.0 km

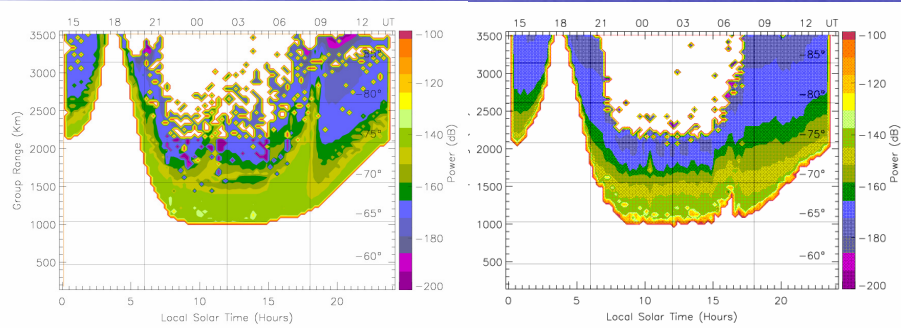




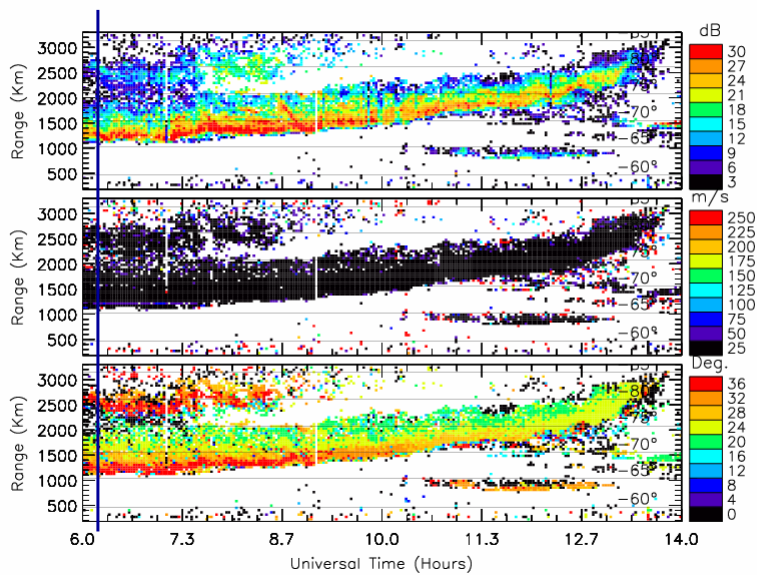
Synthesized TIGER Sea echoes during Spring of 2000 Divergent Power Loss along Beam 4 for 12.0 MHz



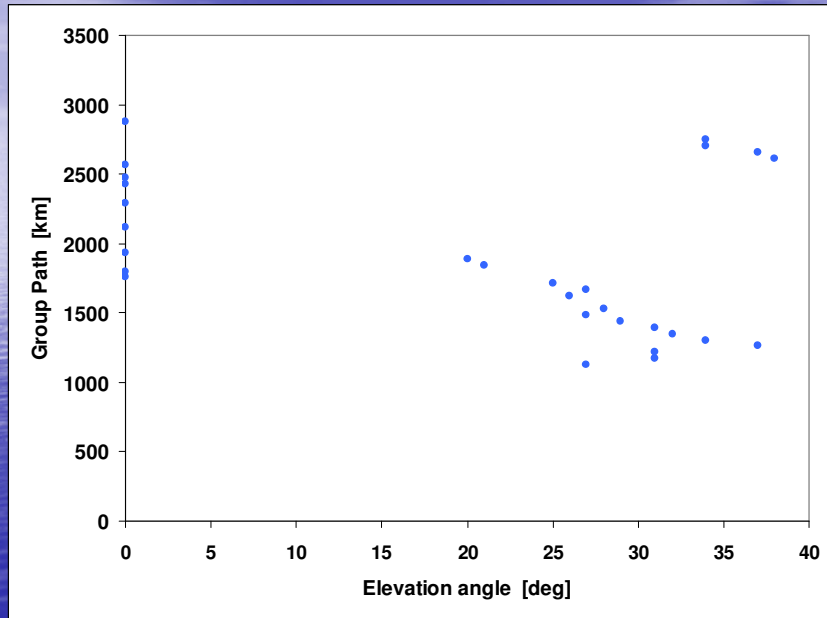
Synthesized TIGER Sea echoes during Spring of 2000 Divergent Power Loss along Beam 4 for 12.0 MHz



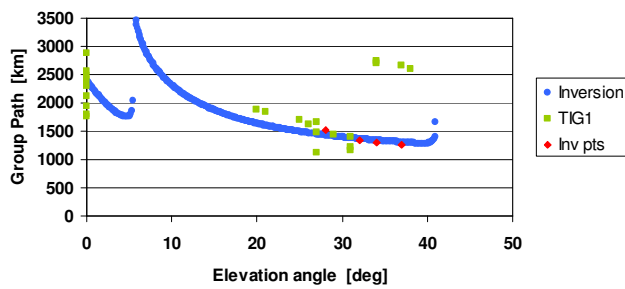
TIGER Inversion 3/9/2000 12.0MHz



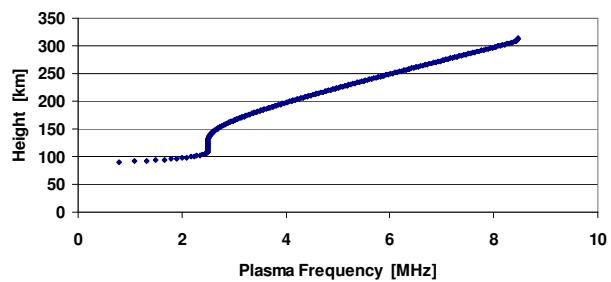
TIGER1 3/9/2001, 6.1555UT, 12.19MHz, Bm 4



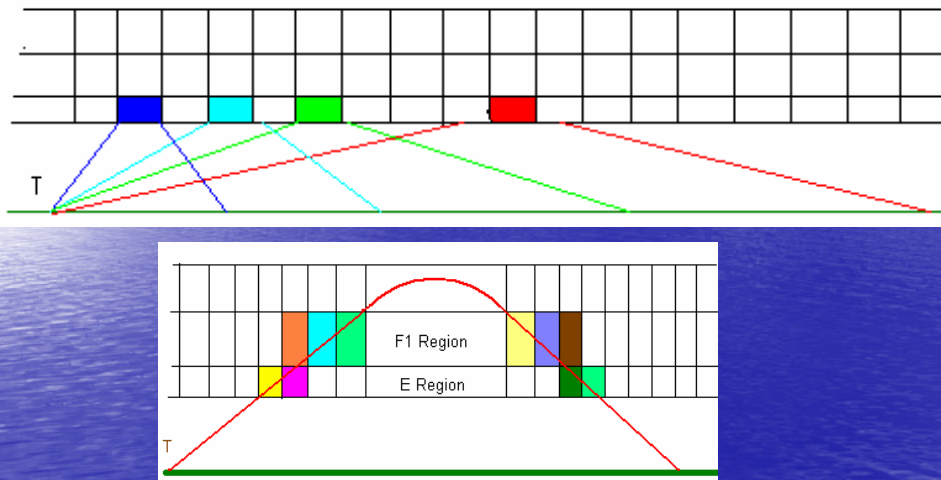
TIGER1 3/9/2000 6.15556UT 12.19 MHz



Ionospheric Profile 3/9/2000 6.15556UT



2-D Smart



Norman RJ, Cannon PS. An evaluation of a new two-dimensional analytic ionospheric ray-tracing technique: segmented method for analytic ray tracing (SMART). *Radio Science*, vol.34, no.2, March-April 1999, pp.489-99.

Future Work to obtain a Grid point ionospheric model/Map

- Model/Map the E layer using a range of frequencies
- 2-D SMART in conjunction with this New Inversion technique
- Model/Map the F1 layer
- Model/Map the F2 layer
- Do for each beam

Acknowledgements

This research was supported by:

- USAF AOARD (Asian Office of Aerospace R&D)

and

- VPAC (Victorian Partnership for Advanced Computing) Expertise Program Grant Scheme.

Appendix 3

Norman R. J., M. L. Parkinson and P.L. Dyson.

Mapping the Ionosphere using a HF Radar Backscatter Inversion Technique.

Proceedings of the Workshop on the Applications of Radio Science, Refereed Paper R-24,
Leura, New South Wales, 15–17 February, 2006.

MAPPING THE IONOSPHERE USING A HF RADAR BACKSCATTER INVERSION TECHNIQUE

R. J. Norman⁽¹⁾, M. L. Parkinson⁽²⁾, and P. L. Dyson⁽³⁾

⁽¹⁾*Department of Physics, La Trobe University, Victoria 3086, Australia*
r.norman@latrobe.edu.au

⁽²⁾*As (1) above, but E-mail: m.parkinson@latrobe.edu.au*

⁽³⁾*As (1) above, but E-mail: p.dyson@latrobe.edu.au*

ABSTRACT

High Frequency (HF) radar land and sea backscatter inversion to obtain ionospheric electron density profiles has the potential to provide remote sensing of the ionosphere up to thousands of kilometers from the transmitter/receiver location. The inversion technique requires HF radar data in the form of time delay or group path, P' , as a function of elevation angle, β , from each of the ionospheric layer echo traces. This HF radar data is inverted to obtain a multiple quasi-parabolic segment (QPS) plasma frequency profile of the true ionosphere. The technique can be used with both fixed frequency and frequency scanning radars. The advantage of using frequency scanning radar is that the down-range gradients in electron density can be determined, and spatial variations of the ionosphere within the radar coverage area can be modeled and mapped. In this paper, a prototype HF radar backscatter inversion technique is exercised using real ionospheric data recorded with the Tasman International Geospace Environment Radar (TIGER).

INTRODUCTION

The inversion technique developed by Norman and Dyson (2005) [1] is applied to real backscatter data from the Tasman International Geospace Environment Radar (TIGER) [2]. TIGER is an Over-the-Horizon Radar (OTHR) situated on Bruny Island (43.4°S, 147.2°E; 55°Λ) and transmits southward toward the austral auroral oval. TIGER was designed to study the physical processes occurring in geospace including the aurora and magnetospheric convection. TIGER is part of the Super Dual Radar Network [3], [4] consisting of 7 radars in the Southern Hemisphere and 10 in the Northern Hemisphere.

TIGER transmits HF signals where some of the signal is reflected from the ionosphere to a distant location on the Earth's surface, which can be up to a few thousand kilometers from the transmitter/receiver location. Some of the signal is reflected back to the transmitter location along the same path via reflection from the ionosphere. The backscattered signals contain useful information regarding the state of the intervening ionosphere at the time, and over the range of the returned signal. Especially strong backscatter from the sea is recorded during the day time, and the elevation angles of the received signals are determined at every group range using an interferometer sub-array [5].

Norman and Dyson [1] describe the backscatter inversion technique in detail where the theory and accuracy of the technique are shown. Their inversion technique requires HF radar data in the form of time delay or group path, P' , as a function of elevation angle, β , from each of the ionospheric layer echo traces. This inversion technique determines quasi-parabolic ionospheric layer parameters [6] for each of the layer echo traces presented in the form of profiles of group path versus elevation angle. At least 3 group path - elevation angle data pairs are required from each layer echo trace, and in general the more data points the better the inversion results will be. The maximum elevation of each of the ionospheric layer echo traces is also a required input, and is used to seed the first guess of the layer parameters. This data is then inverted to form a multiple quasi-parabolic segment (QPS) model ionospheric profile. The QPS model requires 5 QP segments to represent the E, F1, and F2 ionospheric layers.

This research was supported by the USAF AOARD (Asian Office of Aerospace R&D) and VPAC (Victorian Partnership for Advanced Computing) Expertise Program Grant Scheme. The TIGER radar is supported by the Australian Research Council, the Australian Antarctic Science Advisory Council, the Australian Academy of Sciences, and the TIGER Consortium Partners (La Trobe University, Australian Antarctic Division, DSTO Intelligence Surveillance and Reconnaissance Division, IPS Radio and Space Services, Monash University, University of Newcastle).

TIGER has a main array of 16 log-periodic antennas and the use of a phasing matrix permits the main beam to be steered in 16 different directions separated by 3.24° to achieve an azimuthal coverage of $\sim 52^\circ$. TIGER is capable of illuminating the ionosphere over a wide range of elevation angles and azimuth angles. TIGER is frequency agile and in the most common modes of operation automatically selects a frequency appropriate for observations. Once a frequency is chosen, the radar operates at that frequency for extended periods of time. Thus the inversion technique has been developed for a fixed operating frequency. However, by varying the operating frequency of the HF radar it is possible to increase the ionospheric coverage area for the inversion technique and determine the down-range gradients of plasma frequency. Thus the inversion technique can be performed on multi-frequency data collected on each of the 16 beams to construct realistic 3-D mappings of ionospheric electron density.

Norman and Dyson [1] showed an example of the technique using real backscatter data consisting of three ionospheric layer echo traces. Their example used group path versus elevation angle profiles recorded at a single operating frequency. In this paper, the example chosen consists of group path versus elevation angle profiles recorded over a range of operating frequencies, and thus enabling a description of horizontal gradients in the ionosphere to be determined, at least immediately downrange from the radar site. In this initial example, only data recorded on a single beam under relatively simple conditions will be presented to illustrate the capabilities of the technique.

THEORY

The backscatter inversion technique is described in detail in [1] where a QPS model is used to describe the plasma frequency (proportional to the square root of electron density) as a function of the height of the ionosphere near the midpoint of the propagation path. The model is constructed from the backscattered signal from each of the layer echo traces, which are in the form of group path versus elevation angle profiles.

Up to 5 QP segments are required to represent a typical daytime ionosphere. Three of the QP segments represent the 3 ionospheric layers, namely the E, F1 and F2 layers, and 2 QP segments are joining segments between the layers and smoothly attach to the layer QP segments. A QP layer consists of only 3 layer parameters, namely the peak plasma frequency of the layer, the height of maximum electron density of the layer, and the semi-thickness of the layer.

In this paper, the inversion technique is used on a backscatter ionogram example containing a section of echo trace identified as single F-region layer echo trace. Thus the inversion technique will produce results showing a single QP segment. The backscatter ionogram provides the group path versus elevation angle for a range of operating frequencies. By applying the inversion technique on the group path versus elevation angles at each operating frequency, the down-range ionospheric profile can be modeled and mapped.

The inversion technique requires at least three data points in the form of group path versus elevation angle from each of the layer echo traces. The maximum elevation angle of each of the layer echo traces, β_{\max} , is a required input and is used to seed the initial guess ionospheric ray parameters (f_c, r_b, r_m) . The seed values of r_m and r_b can be incremented so that the process homes in to the best possible solution.

The seed layer parameters are then substituted into analytic expressions for the group path where the computed group paths, $P'_{c1}, P'_{c2}, \dots, P'_{cn}$ will most likely differ from the real values P'_1, P'_2, \dots, P'_n . Let the corresponding differences between the real and computed values be $\Delta P'_1, \Delta P'_2, \dots, \Delta P'_n$, respectively. Then, to a first approximation the amount $\delta x_i \equiv (\Delta f_c, \Delta r_b, \Delta r_m)$ by which the assumed layer parameters should be incremented, so that $\Delta P'_1, \Delta P'_2, \dots, \Delta P'_n$ are minimised, is given by

$$\Delta P'(f) = \sum_i \frac{\partial P'(f)}{\partial x_i} \delta x_i$$

Using the same notation as [5] the equation can be re-written in matrix form:

$$|\Delta P'| = \left[\frac{\partial P'}{\partial x_i} \right] |\delta x_i|$$

or as

$$\begin{bmatrix} \Delta P'_1 \\ \Delta P'_2 \\ \vdots \\ \Delta P'_n \end{bmatrix} = \begin{bmatrix} \left(\frac{\partial P'}{\partial r_b} \right)_{\beta_1} & \left(\frac{\partial P'}{\partial r_m} \right)_{\beta_1} & \left(\frac{\partial P'}{\partial f_c} \right)_{\beta_1} \\ \left(\frac{\partial P'}{\partial r_b} \right)_{\beta_2} & \left(\frac{\partial P'}{\partial r_m} \right)_{\beta_2} & \left(\frac{\partial P'}{\partial f_c} \right)_{\beta_2} \\ \vdots & \vdots & \vdots \\ \left(\frac{\partial P'}{\partial r_b} \right)_{\beta_n} & \left(\frac{\partial P'}{\partial r_m} \right)_{\beta_n} & \left(\frac{\partial P'}{\partial f_c} \right)_{\beta_n} \end{bmatrix}^{-1} \begin{bmatrix} \Delta r_b \\ \Delta r_m \\ \Delta f_c \end{bmatrix}$$

or more simply as $Z = S T$

where

$$\begin{aligned} Z &= [\Delta P'] && \text{is a (1, n) matrix,} \\ S &= \left[\frac{\partial P'}{\partial x_i} \right] && \text{is a (3, n) matrix,} \\ T &= [\delta x_i] && \text{is a (3, 1) matrix.} \end{aligned}$$

The inversion of this equation is $T = [S_T S]^{-1} S_T Z$

It should be noted that these equations may be found in [1] where S_T is the transpose matrix of S and the matrix $S_T S$ is a square matrix capable of inversion.

The assumed layer parameter values are then incremented by Δf_c , Δr_b and Δr_m . Thus a new set of layer parameters is determined. The process is repeated until a set of values for the layer parameters produces group path values, which yield to within a specified accuracy, to the chosen real group path versus elevation angle data points.

Using multiple operating frequencies the inversion technique can be applied to data points received from each frequency highlighting different regions of the ionosphere. An overall mapping of the ionosphere in the coverage area of the radar can then be performed.

TIGER RESULTS

Fig. 1 is a TIGER backscatter ionogram recorded on the magnetic meridian pointing beam 4 commencing at 21:00 UT on 20th February 2000. The backscatter ionogram displays the signal-to-noise ratio (SNR) of the received signal in dB versus transmitter frequency and group range. The group range, or group path, is obtained from the time delay of the echo, converted to a distance assuming propagation at the speed of light in a vacuum. TIGER was scanning in frequency from 8 to 20 MHz in steps of approximately 0.1 MHz. The integration time was 3 s per frequency; hence the backscatter ionogram took 6 minutes to acquire. The SNR values were recorded at steps of 45 km using Gaussian-like pulses of width 300 μ s, equivalent to 45 km in range.

SuperDARN radars also measure the line-of-sight Doppler velocity, spectral widths, and elevation angles of echoes [4]. Figs. 2 to 4 are the corresponding backscatter ionograms showing these parameters. A real time radar algorithm automatically tags echoes as emanating from the ground or sea if they have small Doppler speed and spectral width, within certain error limits. The main echo trace which dominates the ionograms has Doppler speeds and spectral widths less than $\sim 15 \text{ m s}^{-1}$, and thus represents 1-hop F-region backscatter from the Southern Ocean. On the other hand, the echo trace with high Doppler speed from 12–13 MHz and 2300–2800 km represents 1.5-hop backscatter from a patch of ionospheric irregularities.

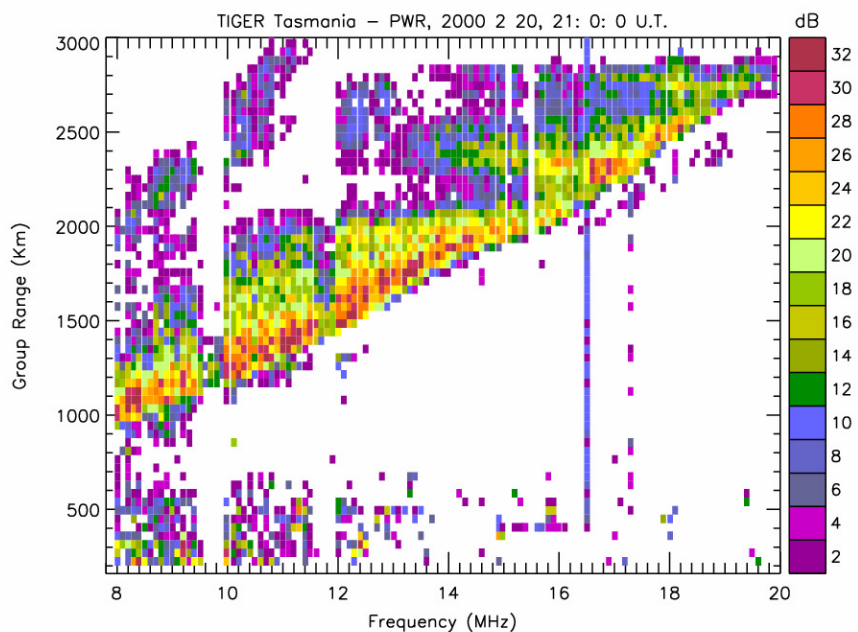


Fig. 1. OTHR ionogram showing the backscatter power (SNR) recorded on TIGER beam 4 at 21:00 UT (07:00 LT) on the 20th February 2000.

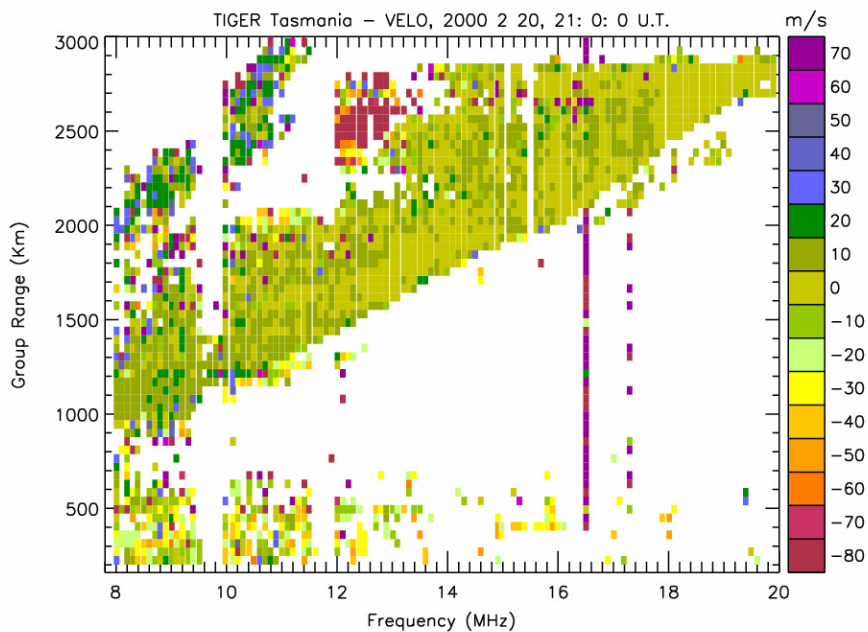


Fig. 2. The same as Fig. 1 except the backscatter ionogram shows the LOS Doppler velocity.

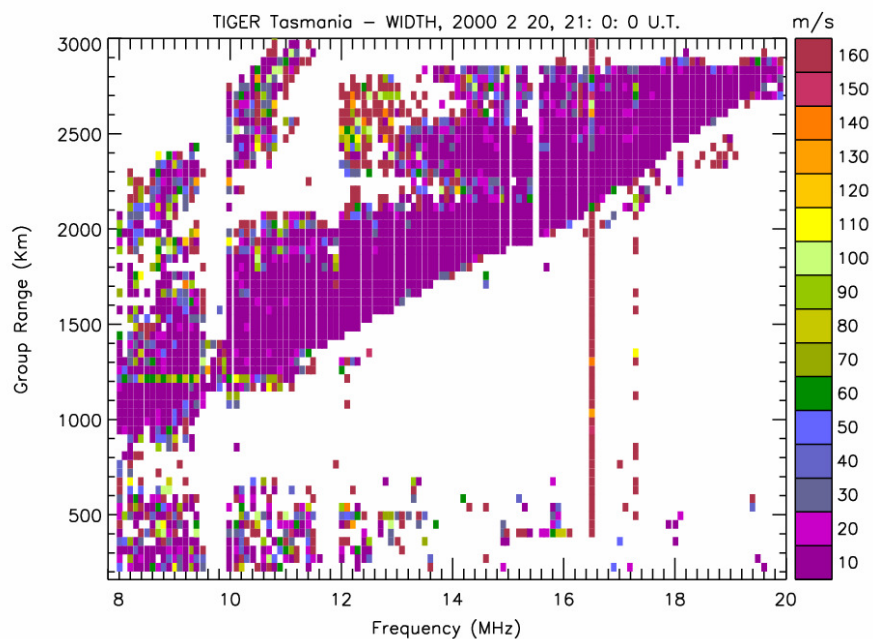


Fig. 3. The same as Fig. 1 except the backscatter ionogram shows the Doppler spectral widths.

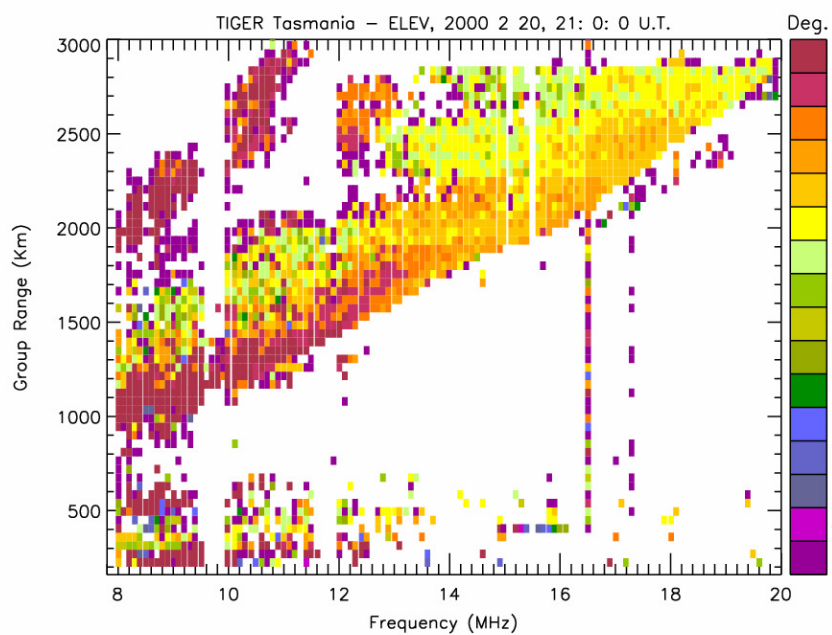


Fig. 4. The same as Fig. 1 except the backscatter ionogram shows the elevation angles.

Both Figures 1 and 4 show that there is complicated structure in the echo traces beyond 2000 km in range. There is an echo trace that starts at about 12 MHz with a leading edge at about 2200 km range. At higher frequencies the signals are stronger and this trace merges with the main trace whose leading edge increases linearly with frequency. This echo structure suggests that there was a dramatic change in the structure of the ionosphere at around 2000 km distant from the radar. The form of the inversion technique presented here assumes that the ray paths associated with sea scatter are symmetric to first order, so it will not give a good representation of sharp, almost discontinuous gradients, which may be associated with the occurrence of the additional echo trace beyond 2000 km range. A more sophisticated inversion method that could deal with such structures was described by Norman and Dyson (2005) which requires the Segment Method Analytic Ray Tracing SMART technique [7 & 8]. Consequently for our purpose here of demonstrating the basic inversion technique, the analysis has been limited to the main F layer trace up to a frequency of 14 MHz.

INVERSION RESULTS

Fig. 5 represents the resultant structure of the ionosphere along the magnetic meridian pointing beam 4 when the group path versus elevation angle profiles contained within the main F layer trace in the backscatter ionogram, Fig. 4, were fed into the inversion program. The plot shows the plasma frequency in kHz versus the ground range and true height. The exact value of the height of the peak electron density, $h_m F2$, has been highlighted using bold horizontal bars, and the numbers located just beneath the base of the F layer represent every fourth value of the operating frequency in kHz. A simple Chapman layer was included to describe the ionosphere above $h_m F2$.

The Fig. 5 results have been pixilated using a nominal resolution of 1 km in true height, and the width in ground range is variable but controlled by the step size used in the frequency scan. The inversion applied to a single frequency yields a vertical profile of the ionosphere nominally located near to the mid-point of refraction, but it is actually related to a significant spread of range determined by oblique propagation through the various layers of the ionosphere. We are in the process of quantifying this effect which will depend on the details of the inversion procedure.

In the absence of low frequency measurements providing group range versus elevation angle data points for the E layer, a simple model E layer was included in the inversion. The chosen parameters were $f_o E = 2.5$ MHz, $h_m E = 115$ km, and a semi-thickness, $y_m E = 15$ km. The E-layer parameters were not varied with ground range, but in principle they could have been by obtaining values from a standard ionospheric model. The main effect of including an E layer in the inversion was to reduce $h_m F2$ for the F layer, especially at the furthest ranges. Increasing the peak density and semi-thickness of the E-layer would reduce $h_m F2$ further than shown here.

Fig. 5 shows how both $h_m F2$ and the peak electron density of the F layer, $f_o F2$, fluctuated with ground range, but overall they increased further away from the radar. At ground ranges < 400 km, $h_m F2$ was ~ 270 km and $f_o F2$ was ~ 6.3 MHz and increasing. At the furthest ground ranges > 1200 km, $h_m F2$ reached ~ 440 km and $f_o F2$ reached > 9 MHz. The ionosphere at furthest ranges was unusually high and dense, and the reality of down-range gradient needs direct, independent corroboration.

The Australian Space Weather Agency (<http://www.ips.gov.au>) operates ionosondes at Hobart (42.9°S, 147.3°E), located close to the TIGER radar site (43.4°S, 147.2°E), and at Macquarie Island (54.5°S, 158.9°E; $-65^\circ\Lambda$), located downrange and just to the east of the TIGER radar field of view. The geomagnetic (geographic) latitude of Macquarie Island corresponds to a ground range of ~ 1035 km on TIGER beam 4, but is separated by a great circle distance of ~ 1010 km. The distribution of plasma density will be partly controlled by electrodynamics and solar illumination at auroral latitudes.

The Hobart and Macquarie Island ionosondes recorded hourly values of $f_o F2 = 6.3$ MHz and 7.3 MHz, respectively, at 21:00 UT on 20 February 2000 (see http://www.ips.gov.au/World_Data_Centre/1/2). In Fig. 5, $f_o F2$ was ~ 6.3 MHz at the closest ground ranges, in agreement with the Hobart ionosonde. However, $f_o F2$ varied between ~ 8 to 9 MHz at ground ranges 1000 to 1300 km. Hence the down-range increase of plasma density was greater than implied by the ionosonde data. However, Macquarie Island was located far away from beam 4, and large, dynamic variations in plasma density are expected at auroral latitudes. Although the IRI model is not accurate at these latitudes, it indicates that $h_m F2$ should have steadily increased with latitude, but only from ~ 273 to 280 km over the ground range shown in Fig. 5.

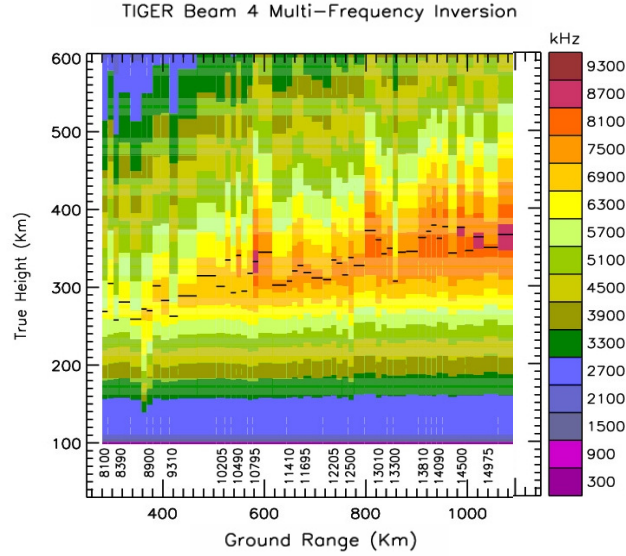


Fig. 5. The down-range variation of ionospheric plasma frequency determined by inverting the backscatter ionogram data recorded on TIGER beam 4 at 21:00 UT (07:00 LT) on the 20th February 2000.

No E-layer parameters were available for the Hobart and Macquarie Island ionosondes at 21:00 UT on 20 February, but on the preceding day, f_oE was 2.65 MHz and 2.85 MHz at the two stations, respectively. Including a uniform model E region with $f_oE=2.5$ MHz in the inversion was conservative, and this may partly account for the large values of h_mF2 and f_oF2 obtained at the furthest ranges.

TIGER observes a remote and poorly known region of the Earth's ionosphere, so development of this technique would provide valuable new, routine information on the electron density structure. Fig 5 shows an increase in f_oF2 with latitude, i.e. distance from the radar. We note that Horvath and Essex [9] also found the electron density to increase with latitude in this region. They analyzed total electron content (TEC) measurements and discovered a dramatic “build up of ionization” located just equator ward of the daytime main ionospheric trough.

The inversion algorithm can quickly home in on layer parameters with a precision far exceeding that obtainable from observations [1]. The errors in the inversion are probably dominated by errors in the measured group range versus elevation angle profiles. Only the 4 group path versus elevation data points with maximum SNR were automatically chosen at each operating frequency for the present analysis. Random errors in the elevation angle data, combined with the effect of the criteria used to automatically select the data points, probably dominate the fluctuations shown in Fig. 5.

SUMMARY AND FUTURE WORK

This new backscatter inversion technique offers a means of sensing remote areas of the ionosphere where it is difficult to obtain vertical ionograms. The down-range gradients in electron density in the coverage area of a radar network, where the group range versus elevation angle profiles are recorded, can be readily determined using this backscatter inversion technique. The procedure can be fully automated, as it was in the present example, and the resultant ionospheric layer parameters and ray tracing results were obtained in a matter of seconds. Applying the technique to multi-frequency, multi-beam radar measurements, 3-D maps of the ionosphere within the radar coverage area can be obtained.

REFERENCES

- [1] R. J. Norman and P. L. Dyson, "HF radar backscatter inversion technique," Submitted to *Radio Sci.*, 2005.
- [2] P. L. Dyson and J. C. Devlin, "The Tasman International Geospace Environment Radar," *The Physicist* (The Australian Institute of Physics), vol. 37, pp. 48–53, March/April, 2000.
- [3] R. A. Greenwald, K. B. Baker, R. A. Hutchins, and C. Hanuise, "An HF phased-array radar for studying small-scale structure in the high-latitude ionosphere," *Radio Sci.*, vol. 20, pp. 63–79, 1985.
- [4] R. A. Greenwald, et. al., "DARN/SuperDARN: A global view of the dynamics of high-latitude convection," *Space Sci. Rev.*, vol. 71, pp. 761–796, 1995.
- [5] P. L. Dyson, and J. A. Bennett, "A model of the vertical distribution of the electron concentration in the ionosphere and its application to oblique propagation studies", *J. atmos. terr. Phys.*, vol. 50, 1988, pp. 251-262.
- [6] T. A. Croft and H. Hoogasian, "Exact ray calculations in a quasi-parabolic ionosphere", *Radio Sci.*, vol. 3, 1969, pp. 69-74.
- [7] R. J. Norman and P. S. Cannon, "A two-Dimensional Analytic Ray Tracing Technique Accommodating Horizontal Gradients", *Radio Sci.*, vol. 32, 1997, pp. 387-396.
- [8] R. J. Norman and P. S. Cannon, "An evaluation of a new two-dimensional analytic ionospheric ray-tracing technique: segmented method for analytic ray tracing (SMART)", *Radio Science*, vol. 34, 1999, pp. 489-499.
- [9] Horvath I, Essex EA. "Using observations from the GPS and TOPEX satellites to investigate night-time TEC enhancements at mid-latitudes in the southern hemisphere during a low sunspot number period" *Journal of Atmospheric & Solar-Terrestrial Physics*, vol.62, no.5, March 2000, pp.371-91.

Appendix 4

Norman, R. J. and P.L. Dyson.

HF Radar backscatter inversion technique.

Radio Sci., (In Press) January 2006. (Refereed journal publication).

HF radar backscatter inversion technique

R. J. Norman¹ and P. L. Dyson¹

Received 30 August 2005; revised 19 January 2006; accepted 10 February 2006; published XX Month 2006.

[1] Methods of inverting high-frequency radar land and sea backscatter to obtain ionospheric vertical profiles offer an important means of remote sensing the ionosphere up to thousands of kilometers from the transmitter/receiver location. This new inversion technique requires the received elevation angle as well as the time delay or group path of the backscattered signal. The technique can be used with both fixed-frequency and swept-frequency radars. The advantage of using swept-frequency radar is that the downrange gradients in electron density can more readily be determined.

Citation: Norman, R. J., and P. L. Dyson (2006), HF radar backscatter inversion technique, *Radio Sci.*, 41, XXXXXX, doi:10.1029/2005RS003355.

1. Introduction

[2] The case we consider is ground backscatter signals received from distant locations on the Earth's surface via reflection by the ionosphere. Both the transmitted and received signals traverse the ionosphere and these signals contain useful information regarding the state of the intervening ionosphere at the time, and over the range of the returned signal which can be up to a few thousand kilometers from the transmitter/receiver location. In this paper a new HF radar backscatter inversion method is presented. It is similar in concept to that of Rao [1974], Bertel *et al.* [1987], and Norman [2003], where inversion techniques were derived for backscatter ionogram inversion. This new inversion technique requires HF radar data in the form of time delay or group path, P' , as a function of elevation angle, β , from each of the ionospheric layer echo traces. This data is then inverted to form a multiple quasi-parabolic segment ionospheric profile, using the quasi-parabolic segment (QPS) model derived by Dyson and Bennett [1988]. This QPS model uses five QPSs to represent the E , F_1 and F_2 ionospheric layers.

[3] The characteristics of the backscattered echoes depend on the radar system characteristics and ionospheric characteristics as well as the backscattering properties of the ground. Important radar characteristics are the wavelength, pulse length, antenna beam width, antenna gain, and transmitted power. HF radars that utilize ionospheric propagation at oblique incidence are

usually capable of illuminating the ionosphere over a relatively wide range of elevation angles, giving rise to the possibility of ground backscatter being detected over a wide span of ranges. The radar characteristics largely affect the signal strength of echoes and the ionospheric structure determines the P' elevation angle characteristics at each frequency so throughout this investigation we consider only these ionospheric effects. Displays of echoes detected by ionospheric HF radars are commonly called ionograms and here we are primarily concerned with fixed-frequency backscatter ionograms displaying echo traces formed by the variation of P' with elevation angle.

[4] The inversion technique was tested using real backscatter data from the Tasman International Geospace Environment Radar (TIGER) [Dyson and Devlin, 2000]. TIGER is an oblique incidence, ionospheric backscatter radar, designed to study the physical processes occurring in space weather systems such as radio aurora. It is situated on Bruny Island (43.4°S, 147.2°E; 55°Λ) and transmits southward and is part of the Super Dual Radar Network [Greenwald *et al.*, 1985, 1995] consisting of six radars in the Southern Hemisphere and nine in the Northern Hemisphere. Throughout this investigation we concentrate on the ionospheric effects on the propagation; that is, it is assumed that the radar characteristics are known and can be accounted for separately.

[5] This new inversion technique derives quasi-parabolic ionospheric layer parameters from the layer echo traces in the form of group path and elevation angle. At least three group path elevation angle data points are required from each layer echo trace. The maximum elevation of each of the ionospheric layer echo traces is also a required input. The inversion technique is based on using a fixed operating frequency. However, by varying the operating frequency of the HF radar it is

¹Department of Physics, La Trobe University, Bundoora, Victoria, Australia.

possible to determine the downrange ionospheric gradients and thus produce more realistic ionospheric mappings.

2. Quasi-Parabolic Segment QPS Model

[6] The QP layer defined by *Croft and Hoogasian* [1968] is given by

$$N_e = \begin{cases} N_m \left[1 - \left(\frac{r - r_m}{y_m} \right)^2 \left(\frac{r_b}{r} \right)^2 \right], & r_b < r < r_m \left\{ \frac{r_b}{r_b - y_m} \right\}, \\ 0, & \text{otherwise.} \end{cases}$$

where

N_e electron density at a radial distance r from the Earth's center;
 N_m maximum electron density at the radial height r_m ;
 r_b radial base height of the ionospheric layer;
 y_m layer semilayer thickness.

[7] The QPS model, presented in the work of *Dyson and Bennett* [1988], consists of smoothly joined QP segments, where QPSs are used to describe each of the ionospheric layers at and immediately below their peaks, and additional QPSs are used as joining segments that smoothly join together the QP descriptions of the layer peaks. The equations describing the QPS ionospheric model may be written as follows.

[8] The E layer is

$$N_E = a_E - b_E \left(1 - \frac{r_E}{r} \right)^2,$$

the joining layer is

$$N_j = a_E - b_j \left(1 - \frac{r_E}{r} \right)^2,$$

and the F layer is

$$N_F = a_F - b_F \left(1 - \frac{r_F}{r} \right)^2,$$

where $a = N_m$ and $b = N_m (r_b/y_m)^2$ and

$$b_j = -r_F b_F \left(1 - \frac{r_F}{r_c} \right) / r_E \left(1 - \frac{r_E}{r_c} \right),$$

where the joining point, r_c , at which the joining layer connect to the F layer may be written as

$$r_c = \frac{r_F b_F \left(\frac{r_E}{r_c} - 1 \right)}{a_F - a_E + b_F \left(\frac{r_E}{r_c} - 1 \right)}.$$

[9] If an F_1 layer is present then QPS joining layers are used between the F_1 and F_2 QPS layers and between the F_1 and E QPS layers.

[10] The work of *Dyson and Bennett* [1988] provides exact expressions for calculating ray parameters such as the group path, P' , for propagation in a spherically stratified ionosphere consisting of a single QP layer. The equation for calculating the group path may be written as

$$P' = 2 \left[\int_{r_o}^{r_b} \frac{r dr}{r \sqrt{r^2 - r_o^2 \cos^2 \beta}} + \int_{r_b}^{r_t} \frac{r dr}{\sqrt{Ar^2 + Br + C}} \right], \quad (1)$$

where r_t is the radial height, from the Earth's center, at which the ray is reflected and

$$r_o^2 \mu^2 - r_o^2 \cos^2 \beta = Ar^2 + Br + C,$$

where μ is the refractive index and β is the elevation angle.

[11] *Dyson and Bennett* [1988] presented explicit equations for the ray parameters in their QPS model for a spherically stratified ionosphere, where if the ray propagates through n segments the group path may be written as

$$P' = 2 \left[\sqrt{r_b^2 - r_o^2 \cos^2 \beta} - r_o \sin \beta + \sum_n (U_n - L_n) \right],$$

where U_n and L_n represent the values of the integral in equation (1) at the upper and lower bounds.

3. New Radar Backscatter Inversion Technique

[12] The method of inversion of the backscattered echo traces presented here requires the determination of the three layer parameters for each of the quasi-parabolic layers, namely the critical frequency f_c , base height r_b , and height of maximum electron density r_m .

[13] The inversion technique begins with inversion of the backscattered signal refracted from the E layer. Once the parameters for the E layer have been calculated the inversion technique inverts the F_1 layer echo trace using the E layer parameter results as well as the QPS equations for the joining layer, which smoothly joins the E layer and the F_1 layer. The process is then repeated for the F_2 layer where the layer parameters already determined for the E and F_1 layers, as well as the equations for the joining layer that joins the F_1 and F_2 layers are required for the inversion process.

[14] The inversion technique requires n (where n is at least 3) data points from each of the layer echo traces, where the n group paths chosen P'_1, P'_2, \dots, P'_n correspond

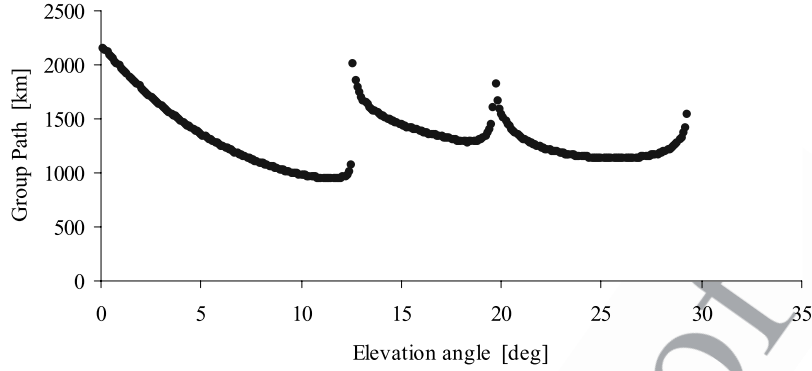


Figure 1. Synthesized group path versus elevation plot using the three-layer ionospheric model with the layer parameters given in the text.

to the n elevations $\beta_1, \beta_2 \dots \beta_n$, respectively. The method then sets out to find a set of values for the layer parameters, which yield to within a specified accuracy, to the data points chosen. To accomplish this an initial guess of the ray parameters (r_c, r_b, r_m) is made.

[15] The maximum elevation angle of each of the layer echo traces, β_{\max} is a required input and is used to determine the initial guess ionospheric parameters and aids in stabilizing the technique. A raypath having an elevation angle of β_{\max} reaches an apogee height equal to the peak height, or maximum height, r_m of the layer. Raypaths with elevation angles greater than β_{\max} penetrate the ionospheric layer.

[16] Then, using the maximum elevation angle of the layer echo trace and an educated guess of the peak height

r_m and the base height r_b of the ionospheric layer, the maximum plasma frequency of the layer can be determined using the equation

$$f_c = \sqrt{f^2 \left(1 - \frac{r_o^2}{r_m^2} \cos^2 \beta_{\max} \right)}.$$

The initial guess values of r_m and r_b can be incremented so that the process homes in to the best possible solution.

[17] These new layer parameters are then substituted into the analytic expressions for the group path for the quasi-parabolic layer. Let the computed minimum group paths, which most likely will differ from the real values P'_1, P'_2, \dots, P'_n , be $P'_{c1}, P'_{c2}, \dots, P'_{cn}$, respectively, and the corresponding differences between the real and computed values be $\Delta P'_1, \Delta P'_2, \dots, \Delta P'_n$, respectively. Then, to a first approximation the amount $\delta x_i \equiv (\Delta f_c, \Delta r_b, \Delta r_m)$ by which the assumed layer parameters should be incremented, so that $\Delta P'_1, \Delta P'_2, \dots, \Delta P'_n$ are a minimum is

Table 1. Three Data Points Chosen From Each of the Layer Echo Traces

Data Points	Elevation Angle β_E , deg	Group Path P'_E , km
<i>E Layer</i>		
1	5.0	1361.49009944569
2	7.0	1168.63887920563
3	9.0	1033.35342695743
$\beta_{\max E}$	12.0	
<i>F₁ layer</i>		
1	19.0	1404.10692246982
2	19.2	1348.36189670986
3	19.4	1319.28979088134
$\beta_{\max F1}$	19.7	
<i>F₂ layer</i>		
1	22.0	1238.53947948455
2	23.0	1187.14934478616
3	24.0	1155.70487464130
$\beta_{\max F2}$	29.3	

Table 2. Convergence of the *E* Layer Parameters to the Correct Result After Each Iteration

	<i>E</i> Layer Iteration				
	1	2	3	4	5
foE, MHz	3.253448	3.344400	3.319285	3.319999	3.320000
ymE, km	13.00000	14.53291	13.98480	13.99999	14.00000
hmE, km	91.00000	101.1981	100.9853	101.0000	101.0000
P'_{c1} , km	1255.018	1359.362	1361.448	1361.490	1361.490
P'_{c2} , km	1070.978	1166.943	1168.593	1168.639	1168.639
P'_{c3} , km	943.9176	1031.923	1033.308	1033.353	1033.353
$\Delta P'_1$, km	106.4718	2.12810	4.188E-2 ^a	2.971E-5	2.87E-9
$\Delta P'_2$, km	97.66112	1.69550	4.579E-2	3.412E-5	1.56E-10
$\Delta P'_3$, km	89.43584	1.43042	4.553E-2	3.631E-5	-.39E-9

^aRead 4.188E-2 as 4.188×10^{-2} .

Table 3. Convergence of the F_1 Layer Parameters to the Correct Result After Each Iteration

		F_1 Layer Iteration					
		1	2	3	4	5	6
t3.4	foF1, MHz	4.716269	4.736789	4.744927	4.749492	4.749995	4.750000
t3.5	ymF1, km	30.40000	41.18461	41.70168	42.85851	42.99864	43.00000
t3.6	hmF1, km	152.0000	163.7422	163.7117	163.9681	163.9997	164.0000
t3.7	P'_{c1} , km	1176.024	1329.081	1319.607	1319.270	1319.289	1319.290
t3.8	P'_{c2} , km	1188.481	1363.036	1349.220	1348.374	1348.362	1348.362
t3.9	P'_{c3} , km	1214.872	1437.361	1408.569	1404.416	1404.109	1404.107
t3.10	$\Delta P'_1$, km	143.2662	-9.791348	-0.3176219	1.9871E-2 ^a	3.1598E-4	2.6038E-8
t3.11	$\Delta P'_2$, km	159.8804	-14.67364	-0.8576807	-1.1789E-2	8.8950E-5	-1.318E-9
t3.12	$\Delta P'_3$, km	189.2347	-33.25370	-4.462045	-0.3086568	-2.5437E-3	-2.223E-7

^aRead 1.9871E-2 as 1.9871×10^{-2} .

194 given by (refer also to Bertel *et al.* [1987] and Norman
195 [2003])

$$\Delta P'(f) = \sum_i \frac{\partial P'(f)}{\partial x_i} \delta x_i$$

197 and may be rewritten in matrix form as

$$|\Delta P'| = \left[\frac{\partial P'}{\partial x_i} \right] |dx_i|$$

198 or in expanded form as

$$\begin{bmatrix} \Delta P'_1 \\ \Delta P'_2 \\ \vdots \\ \Delta P'_n \end{bmatrix} = \begin{bmatrix} \left(\frac{\partial P'}{\partial r_b} \right)_{\beta_1} & \left(\frac{\partial P'}{\partial r_m} \right)_{\beta_1} & \left(\frac{\partial P'}{\partial f_c} \right)_{\beta_1} \\ \left(\frac{\partial P'}{\partial r_b} \right)_{\beta_2} & \left(\frac{\partial P'}{\partial r_m} \right)_{\beta_2} & \left(\frac{\partial P'}{\partial f_c} \right)_{\beta_2} \\ \vdots & \vdots & \vdots \\ \left(\frac{\partial P'}{\partial r_b} \right)_{\beta_n} & \left(\frac{\partial P'}{\partial r_m} \right)_{\beta_n} & \left(\frac{\partial P'}{\partial f_c} \right)_{\beta_n} \end{bmatrix}^{-1} \begin{bmatrix} \Delta r_b \\ \Delta r_m \\ \Delta f_c \end{bmatrix}$$

or more simply as $Z = SK$, where

$Z = [\Delta P']$ (1,n) matrix;

$S = \left[\frac{\partial P'}{\partial x_i} \right]$ (3,n) matrix;

$K = [dx_i]$ (3,1) matrix.

[18] The inversion of this equation is $K = [S_T S]^{-1} S_T$ 210
Z, where S_T is the transpose matrix of S and the matrix 211
 $S_T S$ is a square matrix capable of inversion. 212

[19] The assumed layer parameter values are then 213
incremented by Δf_c , Δr_b and Δr_m . The entire procedure 214
begins again with the new layer parameter values until 215
the differences in group path $\Delta P'_1$, $\Delta P'_2$, \dots , $\Delta P'_n$ converge 216
to a small specified minimum, thereby obtaining the final 217
solution of the layer parameters for that ionospheric 218
layer. 219

[20] Once the layer parameters have been calculated 220
the next ionospheric layer parameters are then solved for 221
using the technique above and the layer parameters 222
already determined. For example let us assume, that 223
the E layer parameters r_{bE} , r_E , foE have already been 224
evaluated using the method shown above. The peak 225
elevation angle of the F_1 layer echo trace, $\beta_{\max F1}$, may 226

Table 4. Convergence of the F_2 Layer Parameters to the Correct Result After Each Iteration

		F_2 Layer Iteration				
		1	2	3	4	5
t4.4	foF2, MHz	6.450973	6.450973	6.445580	6.449979	6.450000
t4.5	ymF2, km	54.50000	72.66666	67.77551	67.99893	68.00000
t4.6	hmF2, km	218.0000	218.0000	213.8218	213.9990	214.0000
t4.7	P'_{c1} , km	1414.500	1259.923	1238.608	1238.538	1238.539
t4.8	P'_{c2} , km	1337.601	1208.438	1187.177	1187.148	1187.149
t4.9	P'_{c3} , km	1277.102	1178.111	1155.730	1155.704	1155.705
t4.10	$\Delta P'_1$, km	-175.9608	-21.38345	-6.88078E-2 ^a	1.278789E-3	2.8484237E-8
t4.11	$\Delta P'_2$, km	-150.4515	-21.28879	-2.71656E-2	1.119846E-3	2.0539801E-8
t4.12	$\Delta P'_3$, km	-121.3973	-22.40620	-2.52626E-2	9.308160E-4	1.7825414E-8

^aRead 6.88078E-2 as 6.8807×10^{-2} .

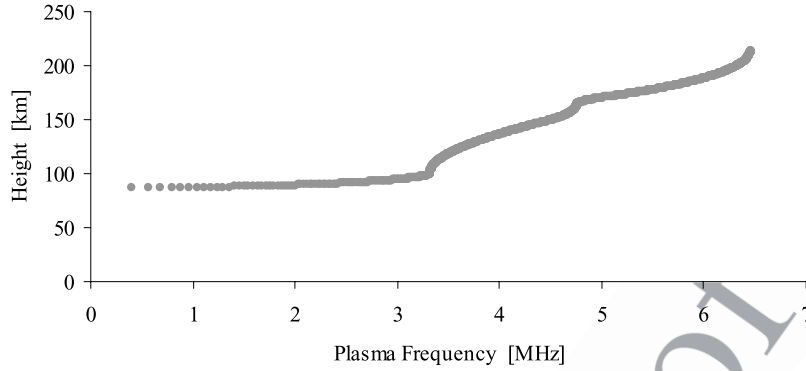


Figure 2. Resultant three-layer ionospheric profile.

be determined directly from the backscattered trace and at least three data points are required from the F_1 layer echo trace. The unknowns to be solved for are $foF1$, r_{bF1} and r_{F1} .

[21] Two additional QP segments are now involved where one represents the joining layer, which smoothly joins the E and F_1 layers and the other QPS representing the F_1 layer from the peak of the F_1 layer down to the point where these two layers are smoothly attached. The joining layer parameters depend on the E and F_1 layer parameters [see *Dyson and Bennett*, 1988]. Thus three QP segments are required to determine the F_1 layer parameters using the inversion technique described here. The equation for the group path in determining the F_1 layer parameters contains the parts of the raypath in (1) the free space (region between transmitter and base of the ionosphere), (2) the QPS representing the E layer, (3) the joining QPS layer joining the E and F_1 layers, and (4) the QPS representing the F_1 layer.

[22] The equation for the group path of the propagated raypaths being reflected from the F_1 layer may be written as

$$P' = 2 \left[\sqrt{r_{bE}^2 - r_o^2 \cos^2 \beta} - r_o \sin \beta + U_E - L_E + U_j - L_j + U_{F1} - L_{F1} \right].$$

[23] Once the F_1 layer parameters are known the F_2 layer parameters may be calculated using the same procedure. In all, up to five QP segments are required to determine the F_2 layer parameters.

4. Inversion of a Synthesized BSI

[24] To test the inversion technique and its stability and inherent accuracy, a synthesized backscatter echo trace with known QP layer parameters was used. The synthesized group path versus elevation angle echo traces,

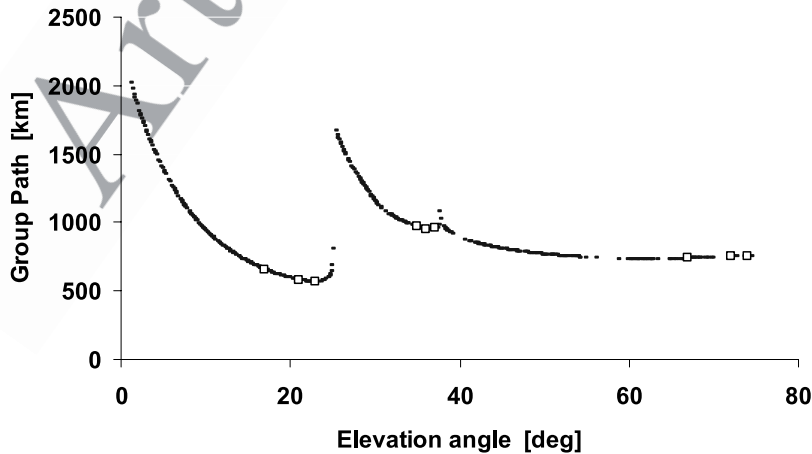


Figure 3. Simulated 3-D numerical ray-tracing results using the IRI ionosphere, where the open squares show the layer echo data points chosen as inputs to the inversion technique.

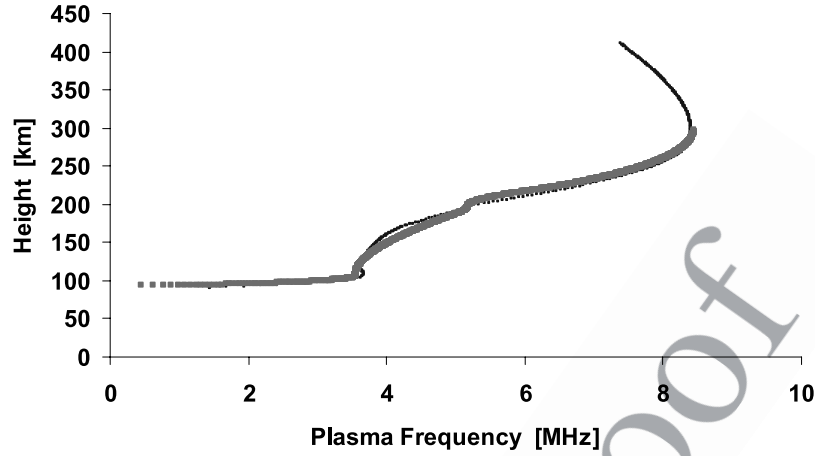


Figure 4. Resultant three-layer ionospheric profile obtained from the inversion technique (thick curve) and the corresponding IRI ionospheric profile at the transmitter location (thin curve).

shown in Figure 1, were determined using an analytic ray-tracing program and the ionospheric layer parameters: $foE = 3.32$ MHz, $y_mE = 14$ km, and $r_E = 101 + r_o$ km (E layer); $foF1 = 4.75$ MHz, $y_m F1 = 43$ km, and $r_{F1} = 164 + r_o$ km (F_1 layer); and $foF2 = 6.45$ MHz, $y_m F2 = 68$ km, $r_{F2} = 214 + r_o$ km (F_2 layer); where $r_o = 6370$ km (the radius of the Earth).

[25] An operating frequency of 12 MHz was used in the determination of the backscattered trace in Figure 1. The layer echo traces are clearly visible where the E layer echo trace is the trace between 0° and 12° elevation, the F_1 layer echo traces is the trace between 12° and 19.7° and the F_2 layer echo trace is between 19.7° and 29.3° elevation. Raypaths for this frequency that have elevation angles greater than 29.3° will penetrate the ionosphere specified by the above layer parameters.

[26] The inversion technique was then applied to this synthesized data. Table 1 shows the three data points chosen from each of the layer echo traces in Figure 1 which is the minimum number of points required for the inversion technique. The maximum elevation angle from each of the layers is also a required input. In this initial

test, high-accuracy input data were used to validate the technique.

[27] The results in Table 2 clearly demonstrate that the inversion technique converges correctly for the first stage of the inversion, that is, the determination of the E layer. After only five iterations the technique has homed into the desired layer parameters. The error in group path between the computed and true values in group path is negligible after only five iterations.

[28] The results in Table 3 clearly demonstrate that the inversion technique converges correctly for the second stage of the processes determining the F_1 layer parameters. After only six iterations the technique has homed into the desired F_1 layer parameters. The difference in group path after only six iterations is negligible.

[29] The results in Table 4 also show that the inversion technique converges correctly in the final stage of the inversion as after only five iterations the technique has homed into the desired F_2 layer parameters. The difference in group path after only five iterations is again negligible.

[30] Tables 2–4 clearly validate the inversion method by showing that the new computed layer parameters converge closer to the true values after each iteration. Figure 2 shows

Table 5. E Layer After Five Iterations^a

P' , km	Error in P' , km
652.8505	4.81E-7 ^b
579.0269	2.81E-7
568.1541	3.55E-6

^aFor the E layer, $foE = 3.55$ MHz, $y_mE = 12.62$ km, and $hmE = 106.08$ km.

^bRead 64.81E-7 as 4.81×10^{-7} .

Table 6. F_1 Layer After Four Iterations^a

P' , km	Error in P' , km
966.5592	-5.59
953.9551	-7.85
955.6044	3.39

^aFor the F_1 layer, $foF1 = 5.17$ MHz, $y_m F1 = 37.74$ km, and $hmF1 = 196.99$ km.

t7.1 **.Table 7.** F_2 Layer After Nine Iterations^a

t7.2	P' , km	Error in P' , km
t7.3	737.4628	-1.61E-9
t7.4	747.9417	-2.08E-9
t7.5	753.5186	-1.91E-9

t7.6 ^aFor the F_2 layer, foF2 = 8.44 MHz, ymF2 = 112.91 km, and hmF2 = 296.56 km.

^bRead 1.61E-9 as 1.61×10^{-9} .

305 the three-layer ionospheric profile having the resultant
306 layer parameters.

307 5. Inversion of Synthesized 308 Three-Dimensional Ray-Tracing 309 Results Using the IRI Model

310 [31] The backscatter results in Figure 3 show synthe-
311 sized one-hop sea scatter using a frequency of 8 MHz
312 where each point corresponds to a ray tube determined
313 from the three-dimensional (3-D) numerical ray-tracing
314 program HIRT (Homing-In Ray Tracing) [Norman *et al.*,
315 1994]. The International Reference Ionosphere (IRI)
316 model [Bilitza, 2001] was used to provide a 3-D repre-
317 sentation of the Earth's ionosphere. The IRI settings
318 were: year 2000; day 50 (local summer); time 1100 LT;
319 geographic transmitter coordinates (43.4°S, 147.2°E;
320 55°A) corresponding to the TIGER SuperDARN radar
321 at Bruny Island, Tasmania, Australia. The synthesized
322 raypaths are determined in the direction of the south
323 geomagnetic pole. The squares in Figure 3 represent the
324 points chosen for the inversion technique.

[32] Figure 4 compares the resultant three-layer iono- 325
spheric profile obtained from the inversion technique 326
(thicker line) with the thin curve representing the IRI 327
ionospheric profile at the transmitter location. These 328
results clearly show that this new inversion technique 329
produces accurate results. The results below highlight the 330
three sets of layer parameters representing the E , F_1 and 331
 F_2 ionospheric layers determined from the inversion 332
technique using the data points represented by the 333
squares from Figure 3 and the small number of iterations 334
required as well as the high level of numerical accuracy 335
obtained (Tables 5, 6, and 7) 336

[33] The results in Figure 5 compare the analytic ray- 337
tracing results obtained using the three layer parameters 338
determined from the inversion process (light diamond 339
points) with the 3-D numerical ray-tracing results 340
obtained using the IRI model (dark dashed points). 341
The data represented by the squares show the values 342
used for the inversion. It is only in the low-angle F_1 343
and F_2 layer echo traces where there is a significant 344
difference in results. Ray tracing shows that there is 345
considerable spreading of the ray tubes reflected at 346
these levels and this causing the signals to be weak 347
and unlikely to be important for propagation experi- 348
ments or communications. 349

6. Example Using Real Other Data 350

[34] The inversion technique was tested using real 351
backscatter data from the Tasman International Geospace 352
Environment Radar TIGER [Dyson and Devlin, 2000]. 353
The TIGER data used is from 29 February 2000 at 354
1200 LT and an operating frequency of 13.095 MHz. 355

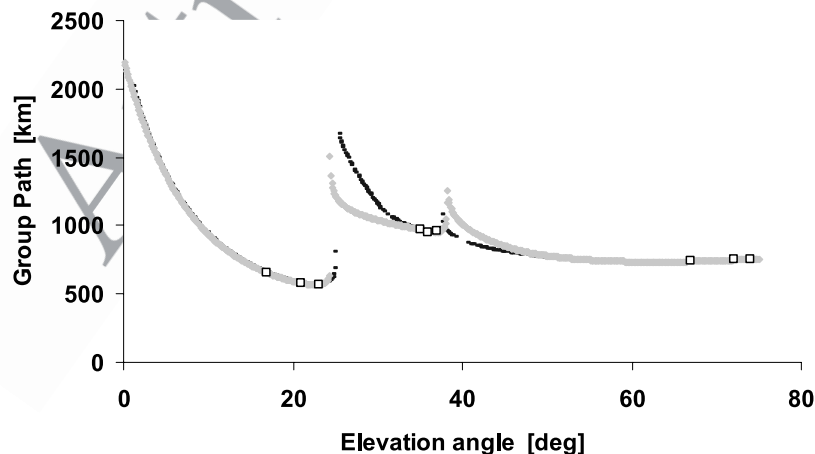


Figure 5. Resultant three-layer analytic ray-tracing results obtained using the parameters determined using the inversion technique (gray diamonds) and the corresponding 3-D numerical ray-tracing results using the IRI model (solid squares). The open squares represent the input data points chosen for the inversion process.

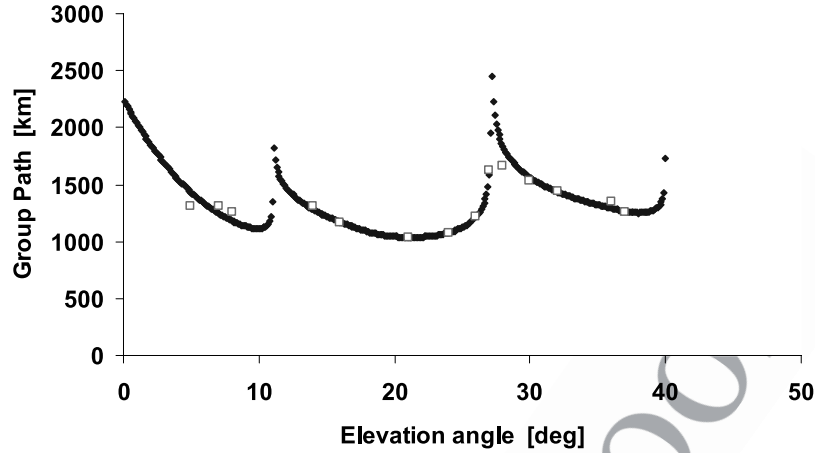


Figure 6. TIGER data points for the inversion process (open squares) and the resultant three-layer analytic ray-tracing results obtained using the parameters determined by the inversion technique (diamonds).

The square data points in Figure 6 represent the back-scattered results received from TIGER and these are the data points used in the inversion program to produce the following ionospheric layer parameters: $f_oE = 3.41$ MHz, $y_m E = 17.8$ km, and $r_E = 107.0 + r_o$ km (E layer); $f_oF1 = 6.60$ MHz, $y_m F1 = 84.4$ km, and $r_{F1} = 197.5 + r_o$ km ($F1$ layer); and $f_oF2 = 6.90$ MHz, $y_m F2 = 55.9$ km, and $r_{F2} = 279.5 + r_o$ km ($F2$ layer); where $r_o = 6370$ km (the radius of the Earth).

[35] Figure 7 shows the ionospheric profile obtained by inversion and represented by the above layer parameters. The diamonds in Figure 6 represent analytic ray-tracing results obtained using the inverted profile shown

in Figure 7. The data points match up well with the synthesized results. It is only in the E layer where there is a difference between the synthesized layer echo trace and the real data.

7. Mapping/Modeling the Ionosphere

[36] The previous examples show that a spherically stratified three-layer model representation of the ionosphere in the region of the radar can be determined using the inversion technique. It will now be shown how this new inversion technique can be used to determine a 3-D

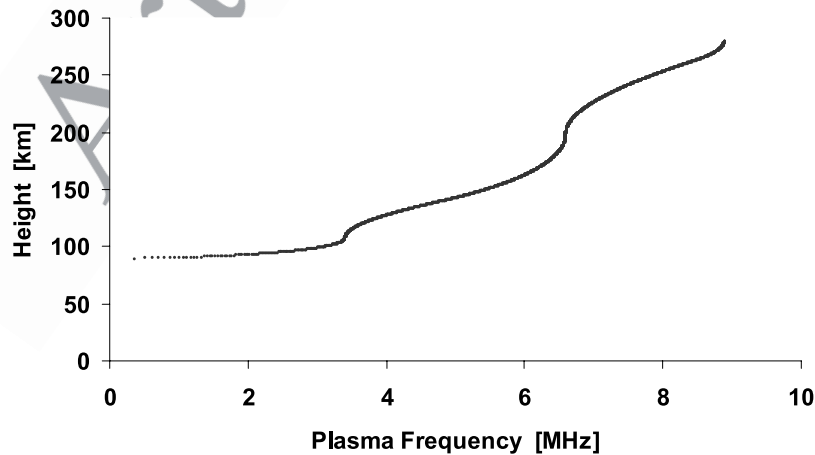


Figure 7. Resultant three-layer ionospheric profile obtained from the inversion of the TIGER backscattered data.

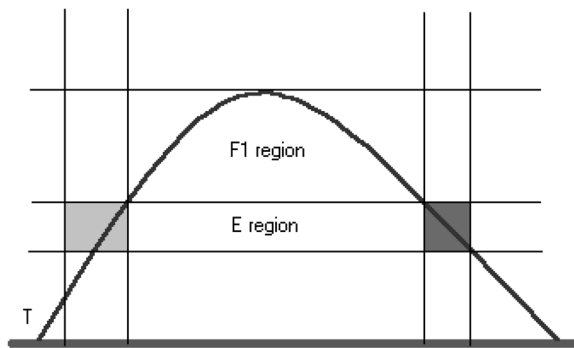


Figure 8. Raypath with an apogee height in the F_1 region of the ionosphere. The ray passes through two different E layers, represented by the light gray and dark gray grid point locations.

grid point model of the ionosphere. The inversion technique described above assumes that the ionosphere is horizontally stratified over the region traversed by the signals used in the analysis. However, if horizontal gradients exist, different raypaths will be affected differently and this will limit the accuracy of the profile obtained by the inversion technique described here.

[37] On the other hand, it is possible to determine the horizontal ionospheric gradients in the coverage area of the radar by applying the inversion technique to results obtained at a number of different radar operating frequencies. Raypaths with different frequencies will be reflected from different regions of the ionosphere. For example, raypaths with frequencies of, say, 8 MHz will in general be reflected from the E layer at ranges closer to the transmitter and with higher elevation angles than raypaths having a frequency of, say, 12 MHz. By stepping through the radar operating frequencies and determining the E layer parameters at each frequency, it is possible using the inversion technique, to determine the E layer parameters at specified range bins, in the direction of the propagated signal, from the transmitter location.

[38] Once having obtained a grid point map/model of the E layer in this way, the F_1 layer can then be similarly mapped/modelled. The raypaths reflected from the F_1 layer will have passed through the E region at two different ranges, as shown in Figure 8. The F_1 layer parameters can then be determined using the inversion technique and the appropriate two sets of E region layer parameters determined in the analysis of the E region data. By stepping through in frequency the F_1 layer parameters can be determined at each specified range bin. Similarly the same process can be applied for the raypaths reflected from the F_2 layer where these raypaths will have passed through each of the F_1 and E regions at

two different ranges. The F_2 layer parameters can then be determined using the appropriate two sets of E region parameters and two sets of F_1 region parameters.

[39] Note that, as shown in Figures 8 and 9, the range grids define specific regions in height and range such that many raypaths may travel through a single grid component. The Segment Method Analytical Ray Tracing (SMART) technique [Norman and Cannon, 1997, 1999; Cannon and Norman, 1997] which performs analytic ray tracing in a grid point ionosphere is ideal in this situation and can be combined with the inversion technique to produce a better grid point ionospheric map/model and also to perform 2-D analytic ray tracing using this new ionospheric map/model.

[40] Many HF radars consist of multiple beams and this approach can be used for each beam. This means that not only the ionospheric gradients in the direction of the beam can be determined but also the gradients at right angles to the beam. The coverage area of the radar can be divided into a grid consisting of latitude, longitude and altitude, where each grid location will be assigned a set of the layer parameters. Thus obtaining a complete map of the ionosphere in the coverage area is possible. The Segment Method Analytical Ray Tracing (SMART) technique [Norman and Cannon, 1997, 1999; Cannon and Norman, 1997] which has now been upgraded to perform 3-D ray tracing can be used in conjunction with the grid point ionosphere to obtain realistic 3-D ray-tracing results and to compare these results with real radar data.

[41] It should be noted that several other inversion methods have been proposed in the past; for example, Landeau *et al.* [1997] developed a technique known as elevation scan backscatter sounding. Their approach was to apply Bayesian methodology described by Tarantola [2005] to the inverse problem, where they applied it to only a single QP layer representing the F layer of the ionosphere. Caratori and Goutelard [1997] developed a relatively simple technique to determine the spatial ionospheric gradients however it requires the addition of

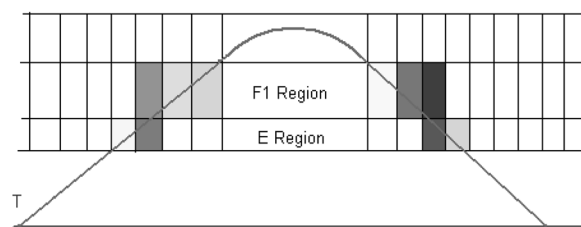


Figure 9. Raypath with apogee height in the F_2 region. The ray passes through a number of different E and F_1 grid point layer representations of the ionosphere.

vertical soundings and the inversion is limited to the F region of the ionosphere.

8. Conclusions

[42] This new inversion technique is robust in that it converges quickly to an accurate result. It has the ability to use many data points from each layer echo trace and in general the more data points used the better the inversion results will be. The technique adds a further dimension to the analysis of HF radars, such as the SuperDARN radar network, where the elevation angle of the received signal is measured and recorded.

[43] **Acknowledgment.** This research was supported by the USAF AOARD (Asian Office of Aerospace R&D) and VPAC (Victorian Partnership for Advanced Computing) Expertise Program Grant Scheme.

References

- Bertel, L., D. Cole, and R. Fleury (1987), The inversion of backscatter ionograms, *IPS Radio Space Serv. Tech. Rep. IPS-TR-88-03*, Sydney, N. S. W., Australia.
- Bilitza, D. (2001), International Reference Ionosphere 2000, *Radio Sci.*, 36, 261–275.
- Cannon, P. S., and R. J. Norman (1997), The relative performance of numeric and analytic ray tracing, in Seventh International Conference on HF Radio Systems and Techniques, *IEE Conf. Publ.*, 441, 145–148.
- Caratori, J., and C. Goutelard (1997), Derivation of horizontal ionospheric gradients from variable azimuth and elevation backscatter ionograms, *Radio Sci.*, 32, 181–190.
- Croft, T. A., and H. Hoogasian (1968), Exact ray calculations in a quasi-parabolic ionosphere, *Radio Sci.*, 3, 69–74.
- Dyson, P. L., and J. A. Bennett (1988), A model of the vertical distribution of the electron concentration in the ionosphere and its application to oblique propagation studies, *J. Atmos. Sol. Terr. Phys.*, 50, 251–262.

- Dyson, P. L., and J. C. Devlin (2000), The Tasman International Geospace Environment Radar, *Physicist*, 37, 48–53.
- Greenwald, R. A., K. B. Baker, R. A. Hutchins, and C. Hanuise (1985), An HF phased-array radar for studying small-scale structure in the high-latitude ionosphere, *Radio Sci.*, 20, 63–79.
- Greenwald, R. A., et al. (1995), DARN/SuperDARN: A global view of the dynamics of high-latitude convection, *Space Sci. Rev.*, 71, 761–796.
- Landeau, T., L. F. Gauthier, and N. Ruelle (1997), Further improvements to the inversion of elevation-scan backscatter sounding data, *J. Atmos. Sol. Terr. Phys.*, 59, 125–138.
- Norman, R. J. (2003), Backscatter ionogram inversion, in *2003 Proceedings of the International Conference on Radar*, pp. 368–374, IEEE Press, Piscataway, N. J.
- Norman, R. J., and P. S. Cannon (1997), A two-dimensional analytic ray tracing technique accommodating horizontal gradients, *Radio Sci.*, 32, 96–387.
- Norman, R. J., and P. S. Cannon (1999), An evaluation of a new two-dimensional analytic ionospheric ray-tracing technique: Segmented method for analytic ray tracing (SMART), *Radio Sci.*, 34, 489–499.
- Norman, R. J., J. A. Bennett, P. L. Dyson, and L. Nguyen (1994), HIRT: Homing-in ray tracing program, research report, School of Phys., La Trobe Univ., Melbourne, Victoria, Australia.
- Rao, N. (1974), Inversion of sweep-frequency sky-wave backscatter leading edge for quasi-parabolic ionospheric layer parameter, *Radio Sci.*, 9, 845–847.
- Tarantola, A. (2005), *Inverse Problem Theory and Methods for Model Parameter Estimation*, chap. 1., pp. 1–40, Soc. for Ind. and Appl. Math, Philadelphia, Pa.

P. L. Dyson and R. J. Norman, Department of Physics, La Trobe University, Bundoora, Vic 3086, Australia. (p.dyson@latrobe.edu.au; r.norman@latrobe.edu.au)